

Multi-Branched Gold Nanoparticles with Intrinsic LAT-1 Targeting Capabilities for Selective Photothermal Therapy of Breast Cancer

Zhan Yuin Ong,^{* † ‡} Shu Chen,[§] Elham Nabavi,[⊥] Anna Regoutz,[§] Alexandra E. Porter,[§] Iain E. Dunlop,[§] David Dexter,^{||} and Daniel Elson[⊥]

[†] School of Physics and Astronomy, University of Leeds, Leeds LS2 9JT, U.K.

[‡] Leeds Institute of Biomedical and Clinical Sciences, School of Medicine, University of Leeds, Leeds LS2 9JT, U.K.

[§] Department of Materials and London Centre for Nanotechnology, Imperial College London, Exhibition Road, London SW7 2AZ, U.K.

[⊥] Hamlyn Centre, Department of Surgery and Cancer, Imperial College London, Exhibition Road, London SW7 2AZ, U. K.

^{||}

* E-mail: z.y.ong@leeds.ac.uk

KEYWORDS. catechol, gold nanoparticle, large neutral amino acid transporter-1, cancer targeting, photothermal

ABSTRACT. Due to the critical role of the large neutral amino acid transporter-1 (LAT-1) in promoting tumor growth and proliferation, it is fast emerging as a highly attractive biomarker for the imaging and treatment of human malignancies, including breast cancer. Whilst multi-branched gold nanoparticles (AuNPs) have emerged as a promising modality in the photothermal therapy (PTT) of cancers, some of the key challenges limiting their clinical translation lies in the need to develop reproducible and cost-effective synthetic methods as well as the selective accumulation of sufficient AuNPs at tumor sites. In this study, we report a direct seed-mediated synthesis of monodispersed multi-branched AuNPs using the catechol-containing LAT-1 ligands, L- and D-dopa, to confer active cancer targeting without the need for additional conjugation with targeting moieties such as peptides or antibodies. Nanoflower-like AuNPs (AuNF) with diameters of approximately 46, 70 and 90 nm were obtained and were found to possess excellent colloidal stability and biocompatibility. A significantly higher cellular accumulation of the L- and D-dopa functionalized AuNFs was observed in a panel of breast cancer cell lines (MCF-7, MDA-MB-231, MDA-MB-468, and MDA-MB-453) when compared to the non-targeting control AuNFs synthesized with dopamine and 4-ethylcatechol. Importantly, no significant difference in uptake between the targeting and non-targeting AuNFs was observed in a non-tumorigenic MCF-10A breast epithelial cell line, hence demonstrating tumor selectivity. For PTT of breast cancer, Ag⁺ was introduced during synthesis to obtain L-dopa functionalized nanourchin-like AuNPs (AuNUs) with strong near infrared (NIR) absorbance. The L-dopa functionalized AuNUs mediated effective photothermal ablation of the triple negative MDA-MB-231 breast cancer cell line as well as sensitized the cells to the anticancer drugs cisplatin and docetaxel. This work may provide new insights on the facile preparation of cancer targeting multi-branched AuNPs with potential for the *in vivo* PTT of breast cancer.

1. Introduction

Breast cancer is the most common cancer among women and is one of the leading causes of morbidity and mortality worldwide.¹ Triple negative breast cancers (TNBCs), in particular, pose a major clinical challenge as they are refractory to the various targeted hormonal therapies available and have a high risk of recurrence.² In recent years, photothermal therapy (PTT) in which light energy is converted into heat, has emerged as a promising treatment modality for the minimally invasive treatment of various cancers such as breast cancer, gastric cancer, head and neck cancer, and melanoma. Anisotropic gold nanoparticles (AuNPs) such as nanorods, nanoprisms, nanostars, and nanoplates have been the focus of intense research as PTT mediators due to their strong localized surface plasmon resonance (LSPR) effect, ease of synthesis and functionalization, excellent biocompatibility, and potential to be simultaneously used as contrast enhancement agents for non-invasive X-ray computed tomography (CT) and photoacoustic imaging.³⁻⁵ Additionally, the longitudinal LSPR peak of anisotropic AuNPs can be readily tuned to the near infrared (NIR) region (650 – 900 nm) to correspond to the biologically transparent window in which tissues and blood minimally absorb. This property enables the use of NIR lasers with deeper light penetration to selectively mediate photothermal ablation of tumors that have taken up the nanoparticles, hence minimizing damage to surrounding tissues. The combination of PTT with conventional chemotherapy has since been proposed as an attractive therapeutic approach to improve antitumor efficacy and minimize side effects.⁴

Despite their promise, one of the key factors limiting the successful clinical translation of AuNP-mediated PTT lies in the poor *in vivo* accumulation of nanoparticles at tumor sites.⁴ AuroShell[®] (Nanospectra Biosciences), which are silica nanoparticles coated with thin PEGylated gold shells, currently represent the only AuNP-based PTT device that has been evaluated in clinical trials.^{4, 6-7} Whilst encouraging patient responses were observed in Phase I

and II clinical trials for recurrent/refractory head and neck cancer, primary and metastatic lung cancer, and prostate cancer, it was found that only 1% of the injected dose achieved tumor accumulation as the nanoparticles relied solely on the enhanced permeation and retention (EPR) effect to passively accumulate in the tumor. It could thus be envisaged that the incorporation of active targeting strategies to increase tumor accumulation of AuNPs could potentially lead to enhanced antitumor effects, less side effects, and reduced treatment costs during PTT. In this regard, numerous researchers have successfully investigated the surface conjugation of pre-synthesized AuNPs with macromolecules such as cell penetrating or targeting peptides, aptamers, antibodies or nanobodies for active targeting to cell surface receptors or molecules that are frequently overexpressed in cancer cells or its microenvironment.⁴ Such approaches, however, often involve time-consuming chemical conjugation, purification, and characterization procedures, as well as the use of expensive cross-linkers, peptides and/or monoclonal antibodies which may not be ideal in the large scale commercial synthesis of AuNPs for clinical use.^{4, 8} The continued development of facile synthetic methods to reproducibly obtain monodispersed cancer targeting AuNPs will therefore be key for their successful clinical translation as effective photothermal agents. At the same time, the targeting of novel receptors or transporters that are consistently overexpressed in different cancer types, staging, and sub-types provides advantages for the broad utility of these novel devices in the selective photothermal ablation of a wide range of malignancies.

The large neutral amino acid transporter 1 (LAT-1) forms a functional heterodimeric complex with 4F2hc (or CD98) heavy chain to transport a wide range of branched or aromatic amino acids and their related drugs such as leucine, phenylalanine, tryptophan, L-dopa, triiodothyronine, and melphalan in a sodium-independent manner.⁹ It plays a crucial role in facilitating amino acid uptake for protein synthesis, metabolic activities, and regulation of

complex signaling pathways in rapidly dividing tumor cells and thus has been found to be overexpressed in the majority of human neoplasms.¹⁰ Particularly in breast cancers, LAT-1 has been found to be frequently overexpressed in tumor cells, with little or no expression in normal mammary ducts or adjacent breast tissues, and its co-expression with 4F2hc is correlated with poor disease prognosis in the triple-negative subtype.¹¹⁻¹² Given its important role in promoting tumor proliferation, the LAT-1 represents a highly attractive, but yet poorly exploited, biomarker for the imaging and treatment of breast cancers.^{11, 13} Recently, the effectiveness of targeting LAT-1 for anticancer drug delivery to breast cancer and glioma was reported by Li *et al.*¹⁴⁻¹⁵ It was demonstrated that the use of LAT-1 targeting glutamate-functionalized polyoxyethylene stearate PLGA nanoparticles to deliver paclitaxel led to significantly higher tumor accumulation and inhibition of tumor growth in a subcutaneous 4T1 breast carcinoma mouse tumor model compared to the non-targeting control nanoparticles.¹⁴

Based on these observations, we hypothesized that the incorporation of LAT-1 targeting moieties on AuNPs would selectively increase nanoparticle accumulation inside tumor cells for the PTT of breast cancer. At the same time, the judicious choice of a reducing-cum-capping agent can simultaneously give rise to multi-branched AuNPs and present the primary amine, carboxylic acid, and bulky side groups that are requisite for interaction with the LAT-1.⁹ This direct synthesis of multi-branched AuNPs is expected to offer significant time and cost savings in the preparation of active targeting AuNPs for PTT. To achieve this, we focused on the seed-mediated synthesis of monodispersed multi-branched AuNPs using the LAT-1 ligands L- and D-dopa as reducing-cum-capping agents to confer intrinsic LAT-1 targeting properties, without the need for additional conjugation steps or the traditional use of cytotoxic surfactants such as cetrimonium bromide. L- and D-dopa belong to the catechol class of compounds which consists of two hydroxyl groups bonded to a benzene ring in the

ortho position. During oxidation, the two hydroxyl groups in the catechol lose four electrons to form quinones and are therefore capable of reducing the AuCl_4^- species to produce gold atoms.¹⁶⁻¹⁷ In this study, in order to improve the uniformity of the synthesized multi-branched AuNPs for PTT, the reduction process was conducted in the presence of pre-formed gold seeds which served as catalysts to promote the reduction of AuCl_4^- by the catechols and enable the selective deposition of gold atoms onto the surface of the metal clusters, thus avoiding secondary nucleation.¹⁸⁻¹⁹ Given the structural similarity of catechols to hydroquinone (another hydroxylated aromatic), it is likely that the former similarly promoted preferential deposition of gold atoms onto the active (111) facets in a kinetically driven manner, thereby giving rise to nanoparticles with a multi-branched nanoflower-like growth.²⁰⁻

²¹ For a valid comparison of active targeting properties, non-targeting AuNPs with comparable multi-branched morphologies were synthesized using dopamine and 4-ethylcatechol, which similarly belong to the catechol class but do not fully possess the functional groups recognized by the LAT-1 (i.e. both α -amino and α -carboxylic acid groups⁹). The cytotoxicities and cellular targeting capabilities of the synthesized AuNPs were first evaluated in a panel of breast cancer cell lines (MCF-7, MDA-MB-231, MDA-MB-468, and MDA-MB-453) and a non-tumorigenic breast epithelial MCF-10A cell line. The functional versatility of this system for PTT was further demonstrated by tuning the LSPR peak of the synthesized AuNPs to the NIR region by exploiting the underpotential deposition effect of silver ions to increase the aspect ratios of the branches,²²⁻²⁴ yielding sea urchin-like AuNPs (AuNUs). The targeted PTT mediated by the AuNUs alone as well as combination with chemotherapeutic drugs cisplatin and docetaxel were investigated in the triple negative MDA-MB-231 metastatic breast cancer cell line. Taken together, this study offers a new perspective on the facile preparation of multi-branched AuNPs with intrinsic LAT-1 targeting capabilities for the photothermal treatment of breast cancer.

2. Experimental Section

2.1. Materials: Gold (III) chloride trihydrate, L-3,4-dihydroxyphenylalanine (L-dopa), dopamine hydrochloride, 4-ethylcatechol, poly(ethylene glycol) methyl ether thiol (mPEG thiol) average Mn 6,000, and silver nitrate were purchased from Sigma Aldrich. D-3,4-dihydroxyphenylalanine (D-dopa) was obtained from Santa Cruz Biotechnology. All reagents were used as received without further purifications. The LIVE/DEAD[®] Viability/Cytotoxicity Kit was purchased from Thermo Fisher Scientific. Milli-Q water (18.2 M Ω ·cm resistivity at 25 °C) was used for the cleaning of glassware and the synthesis of AuNPs.

2.2. Synthesis of AuNPs: *2.2.1. Preparation of Au seeds.* All glassware and stir bars were thoroughly cleaned with aqua regia (HCl:HNO₃, 3:1 v/v) before use. Spherical gold seeds with a diameter of approximately 14 nm were first prepared by adding 300 μ L of 388 mM sodium citrate to 100 mL of boiling 3.0×10^{-1} mM HAuCl₄·3H₂O solution under stirring. The mixture was kept boiling for 15 min until a wine red color was observed. The resultant citrate-capped AuNPs were pelleted by centrifugation (10,016 \times g for 2 h) and rinsed thrice with Milli-Q water to remove excess reagents.

2.2.2. Synthesis of catechol-functionalized nanoflower-like AuNPs (AuNFs). In a typical synthesis of 90 nm catechol-functionalized AuNFs, 100 μ L of 0.1 M HAuCl₄·3H₂O, 144 μ L of 3.8×10^{-1} mM spherical gold seeds, 400 μ L of 1.7 mM mPEG thiol, and 4.0 mL of 15 mM catechol solution were sequentially added to 46.0 mL of Milli-Q water under vigorous stirring. The color of the mixture turned from pale yellow to pink to reddish brown, and finally to bluish brown within 3 min. After allowing the mixture to stir at room temperature for 2 h, the synthesized AuNPs were pelleted at 800 \times g for 10 min, and rinsed at least thrice with Milli-Q water to obtain a dark blue colloidal dispersion. 46 and 70 nm catechol-

functionalized AuNPs were synthesized in a similar manner except with the volume of 0.1 M HAuCl₄·3H₂O solution reduced to 12.5 and 50 μL, respectively.

2.2.3. Synthesis of catechol-functionalized nanourchin-like AuNPs (AuNUs). To synthesize catechol-functionalized AuNUs with a LSPR excitation wavelength in the NIR region, 20 μL of 0.1 M HAuCl₄·3H₂O, 100 μL of 1.0×10^{-1} mM AgNO₃, 28.8 μL of 3.8×10^{-1} mM spherical gold seeds, 80 μL of 1.7 mM mPEG thiol, and 300 μL of 15 mM L-dopa or 4-ethylcatechol were sequentially added to 10 mL of water under vigorous stirring. The reaction was allowed to proceed at room temperature for 2 h, after which the resultant AuNUs were purified as described above.

2.3. Characterization of AuNPs: Synthesized AuNPs were characterized by high resolution TEM (JEOL JEM-2100F) using 200 kV acceleration voltage and by UV-vis-NIR spectrophotometry (Agilent Cary 6000i). Samples were prepared by drying diluted AuNP solutions on holey carbon-coated copper grids. The core diameters, tip-to-tip lengths, and spike aspect ratios of the AuNUs were measured from the TEM images obtained using the ImageJ software. The core diameters and tip-to-tip lengths were measured twice for each AuNU, while four spikes per AuNU were measured from the edge of the core to the tip. The aspect ratio of the spikes were determined by dividing the spike length by the base width of the spikes. The hydrodynamic diameters and zeta-potentials of the AuNPs were measured by dynamic light scattering (DLS) using the Zetasizer Nano (Malvern Instrument Ltd., Worcestershire, UK) equipped with a He-Ne laser. Scattered light was detected at an angle of 173° and at a set temperature of 25 °C. Particle size and zeta-potential measurements were repeated for 3 runs per sample, and reported as the mean ± standard deviation of 3 readings. The nanoparticle concentration of the respective samples equivalent to 1 μg/μL of gold was determined using NanoSight NS300 nanoparticle tracking analysis (NTA) concentration measurement upgrade (Malvern Instrument Ltd., Worcestershire, UK). At least 3 independent

samples per type of functionalized AuNP were analyzed for 3 runs per sample, and reported as the mean \pm standard deviation of 3 readings.

To determine the elemental gold concentration of the synthesized AuNPs, an aliquot of known volume was dissolved in aqua regia, diluted with Milli-Q water, and analyzed using inductively coupled plasma-atomic emission spectroscopy (ICP-AES; Thermo Scientific iCAP 6300 Duo). The surface of the functionalized AuNPs was characterized using a Thermo Scientific K-Alpha⁺ X-ray Photoelectron Spectrometer (XPS) system operating at 2×10^{-9} mbar base pressure. This system incorporates a monochromated, microfocused Al K α X-ray source ($h\nu = 1486.6$ eV) and a 180° double focusing hemispherical analyser with a 2D detector. The X-ray source was operated a 6 mA emission current and 12 kV anode bias. Data were collected at 200 eV pass energy for survey and 20 eV pass energy for core level and valence band spectra using an X-ray spot size of 400 μm^2 . A flood gun was used to minimize sample charging. Spectra were aligned assuming the C 1s core line to be at a binding energy of 285.0 eV and normalized to the Au 4f_{5/2} peak. All data were analyzed using the Avantage software package.

2.4. Cell culture: Human breast cancer cell lines MCF-7 and MDA-MB-231 were maintained in MEM, while MDA-MB-453 and MDA-MB-468 were maintained in DMEM/F12. Both types of cell culture media were supplemented with 10% FBS, 100 U/mL penicillin, and 100 mg/mL streptomycin. Non-tumorigenic immortalized breast epithelial cell line MCF-10A was cultured using DMEM/F12 media supplemented with 5% horse serum, 20 ng/mL EGF, 0.5 mg/mL hydrocortisone, 100 ng/mL Cholera toxin, 10 $\mu\text{g/mL}$ insulin 100 U/mL penicillin, and 100 mg/mL streptomycin. All cell lines were cultured at 37 °C under an atmosphere of 5% CO₂ and 95% humidified air.

2.5. Cytotoxicity testing: The effects of AuNF treatment on cell proliferation was determined using the WST-1 assay. Briefly, MCF-7, MDA-MB-231, and MCF-10A were

seeded onto 96-well plates at a density of 1.2×10^4 cells per well, and allowed to adhere overnight. The cells were then treated with 0, 5, 15, 50, and 100 $\mu\text{g}/\text{mL}$ of Au content for the various AuNFs (46, 70 and 90 nm) for 48 h. Subsequently, the cells were rinsed twice with PBS before 100 μL of growth media and 10 μL of WST-1 reagent were added to each well. The cells were incubated for 3 h at 37 $^\circ\text{C}$ before the absorbance reading were determined at 440 nm using a microplate spectrophotometer. Relative cell proliferation was expressed as $[(A_{\text{sample}} - A_{\text{blank}})/(A_{\text{untreated control}} - A_{\text{blank}})] \times 100\%$. Data are expressed as mean \pm standard deviations of three replicates per concentration.

2.6. Cellular uptake studies: MCF-7, MDA-MB-231, MDA-MB-453, MDA-MB-468, and MCF-10A were respectively seeded onto 12-well plates at a density of 1.8×10^5 , 2.5×10^5 , 2.5×10^5 , 2.5×10^5 , and 1.8×10^5 cells per well, and allowed to adhere overnight. The incubation media in each well was replaced with cell culture media containing 15 $\mu\text{g}/\text{mL}$ Au content for the various AuNFs (46, 70 and 90 nm). After 12 h incubation at 37 $^\circ\text{C}$, non-internalized AuNFs were removed, and the cells were rinsed thoroughly with 1 mL of PBS for 5 times. The cells were then trypsinized, rinsed once with PBS, and pelleted by centrifugation at 1300 \times rpm for 4 min. The cell pellet was digested overnight with 800 μL of aqua regia at room temperature. The respective samples were subsequently diluted with a known volume of Milli-Q water before the analysis of Au content using ICP-AES.

The competition assay was performed by co-incubating MCF-7 cells with 0, 2, and 20 mM of free amino acids phenylalanine or serine and 15 $\mu\text{g}/\text{mL}$ gold content of L-dopa functionalized AuNFs. The cells were co-incubated with free amino acids and the functionalized AuNFs for 5 h before being processed as described above for the analysis of elemental Au content using inductively coupled plasma-mass spectroscopy (ICP-MS; Perkin Elmer ELAN[®] DRC-e).

2.7. Preparation of cell samples for TEM imaging: MDA-MB-231 cells were seeded onto 6-well plates at a density of 6.25×10^5 cells/mL and allowed to adhere overnight. The cells were incubated with 15 $\mu\text{g/mL}$ gold content of L-dopa- and 4-ethylcatechol-functionalized AuNFs for 4 and 12 h. Following incubation, the cells were rinsed thrice with $1 \times$ PBS and fixed with 2% glutaraldehyde and 2% formaldehyde in 0.1M sodium cacodylate (pH 7.4) for 1 h at room temperature. The cells were subsequently stained with 1% osmium tetroxide for 30 min, rinsed thrice with Milli-Q water, and dehydrated in a series of graded ethanol (50%, 70%, 95%, and 100% by volume). Aided by centrifugation, the cells were then infiltrated with increasing concentrations of Epon/acetonitrile resin. The final resin-infiltrated samples were then polymerized at 100 °C for 30 min. The embedded cells were sectioned to a thickness of approximately 50 – 100 nm onto a water bath using an ultra-microtome (Leica EM UC6) equipped with a 35° diamond knife and collected onto 300 mesh copper TEM grids. Multiple cells (> 100 per sample) from triplicate wells per treatment were observed using the high-angle annular dark-field-scanning transmission electron microscope (HAADF-STEM) mode on the FEI Titan 80–300 TEM/STEM operated at 300 kV.

2.8. Photothermal ablation: Human MDA-MB-231 breast cancer cells were seeded at a concentration of 3.5×10^4 cells per well in a 96-well plate and cultured for 48 h. The cell culture media in each well were replaced with fresh media containing 0, 50, and 100 $\mu\text{g/mL}$ Au content of AuNUs and returned to the incubator for three days. Following incubation, non-internalized AuNUs in each well were removed and the cells were rinsed three times with 100 μL of $1 \times$ PBS before 60 μL of phenol red-free MEM containing 10% serum were added to each well. The cells in each well were subsequently subjected to irradiation using an 808 nm continuous wave laser at 9.4 W/cm^2 for 3 min (spot size 0.3 cm^2). After laser exposure, the cells were incubated for a further 24 h at 37 °C before cell viability was determined using the WST-1 assay. To investigate the thermal effects of extracellularly applied AuNUs following

laser treatment, phenol-red free cell culture media containing the respective amounts of AuNUs were added to the cells immediately before laser irradiation. For the LIVE/DEAD[®] viability/cytotoxicity assay, 2.1×10^4 cells per well were seeded into each well of a 4-well chamber slide, and subjected to a similar AuNU treatment and laser exposure protocol as described above, after which the cells were stained with calcein AM and ethidium homodimer-1 for 30 min at room temperature before being imaged under a confocal laser scanning microscope (Leica TCS SP8).

The use of photothermal therapy to sensitize AuNU-treated breast cancer cells to chemotherapy was studied by the addition of cell culture media containing 83.3 μ M cisplatin and 100 nM docetaxel to each well immediately after laser exposure. The cells were incubated with the chemotherapeutic agents for a further 24 h at 37 °C before the WST-1 assay was performed.

2.9. Statistical analysis: The results obtained were analyzed using the two-tailed Student's *t*-test to determine statistical significance (Microsoft Excel). The difference between mean readings was considered to be statistically significant when $P < 0.05$.

3. Results and discussion

3.1. Catechol-mediated synthesis and characterization of nanoflower-like AuNPs (AuNFs). AuNFs were synthesized by first preparing approximately 14 nm gold seeds using the citrate reduction method (Figure S1), followed by the selective reduction of gold ions onto the gold seeds using each of the four different catechols (i.e. L-dopa, D-dopa, dopamine, and 4-ethylcatechol) as a mild reducing-cum-surface capping agent (Figure 1a). Poly(ethylene glycol) methyl ether thiol (mPEG thiol), which binds to the AuNF surface *via* oxidative addition of thiol to Au was included in the synthesis to enhance colloidal stability, biocompatibility, and blood circulation times *in vivo*.²⁵⁻²⁶ The addition of mPEG thiol during

synthesis was indeed found to be essential for obtaining narrowly dispersed AuNPs that were stable during prolonged storage at 4 °C (> 1 year) as well as the ability to be re-dispersed after freeze-drying. As expected in a diffusion-controlled atom addition process on pre-formed metal seeds,²⁷ the addition of increasing amounts of HAuCl₄·3H₂O gave rise to correspondingly larger AuNFs with diameters of approximately 46, 70 and 90 nm (by TEM; Figure 1b, c, and d). As seen from Table S1, the hydrodynamic diameters and zeta-potentials of the synthesized AuNFs ranged from 55.5 to 116.5 nm and -32.6 to -41.0 mV, respectively. Importantly, the synthesized AuNFs possessed narrow size distributions which could be seen from the TEM images (Figure 1b, c, and d) as well as from the small polydispersity indices (PDIs) of ≤ 0.2 obtained from DLS measurements (Table S1). This property is favorable for the reliable and accurate interpretation of biological effects as differently sized nanoparticles within a given formulation may elicit disparate cell interactions and toxicity.²⁸ The synthesized AuNFs gave rise to an intense UV-vis absorption peak ranging from 563 to 649 nm, which red-shifted with size for each functionalization type (Figure S2a).

High resolution TEM (HRTEM) images revealed interplanar distances of approximately 0.233 nm and 0.206 nm, which are close to the characteristic values reported for Au (111) and (200) lattice planes, respectively,²⁹ hence confirming that the multi-branched AuNFs are composed of Au (Figure S3). Additionally, the successful conjugation and presentation of the respective catechols on the surface of the AuNFs was confirmed by XPS analysis. Survey spectra of the 90 nm catechol-functionalized AuNFs showed a strong signal from Au 4f and depending on the catechol, varying signals from C, N and O 1s (Figure S4a). A small amount of Si, which was due to the carrier substrate used, was also observed. For all samples, the Au 4f core level is at a binding energy of 84 eV and shows a spin orbit split of 3.6 eV, both typical for metallic Au (Figure S4b). The C and N 1s core levels are ideal to identify the type of catechol on the surface of the AuNFs. For the C 1s spectrum 3 distinct contributions can be

identified: C-C and C=C environments at 285.0 eV, C-OH and C-NH₂ environments at 286.3 eV, and the carboxylic group at 289.0 eV. AuNFs synthesized using L- and D-dopa were found to possess both carboxylic acid and amino groups, while those prepared with dopamine showed only the expected contributions from the amino group (Figure S4c and d). As expected, both signals were absent in the spectrum obtained for the AuNFs synthesized using 4-ethylcatechol.

To evaluate their colloidal stability, L-dopa functionalized AuNFs were incubated in various biologically relevant media including deionized water, 1 × PBS, cell culture media containing 10% v/v serum, and 100% serum and monitored for changes in hydrodynamic diameters by DLS over time. The AuNFs were incubated at 37 °C with continuous shaking to mimic blood circulation. As seen in Figure S5, the L-dopa-functionalized AuNFs remained stable in deionized water and 1 × PBS, with minimal changes in hydrodynamic diameters, which were approximately 115 and 111 nm, respectively over three days of incubation. Similarly, no shift in the UV-vis absorbance peaks was observed when the AuNFs were dispersed in 1 × PBS (Figure S2b). In serum-containing cell culture media, however, the AuNFs gradually increased in size from 125.9 ± 0.8 nm (t = 0 h) to 167.4 ± 0.5 nm (t = 72 h). A similar observation was made for the AuNFs incubated in 100% serum, with a higher initial diameter of 164.3 ± 2.5 nm at 0 h increasing to 186.0 ± 0.4 nm by 72 h. The increase in hydrodynamic diameters of the AuNFs in serum-containing media and 100% serum could likely be attributed to the passive adsorption of serum proteins onto the nanoparticle surface. Despite the size increment, the hydrodynamic diameter of the AuNFs began to plateau at 72 h; and the resultant size of the AuNFs remained less than 200 nm – a size which still falls within the desired size range for passive tumor accumulation via the EPR effect and the promotion of cellular uptake. In addition to the relatively small sizes observed, the PDIs of the

AuNFs in the different media were also found to remain small (< 0.15) and relatively constant with time, hence suggesting that no uncontrolled aggregation of the AuNFs occurred.

3.2. Synthesis and characterization of sea urchin-like AuNPs (AuNUs) with NIR absorbance. Besides being able to control the size of the AuNFs synthesized using catechols in the seed-mediated approach (Figure 1b-d), the versatility of this system to tune the shape and therefore the LSPR peak of the multi-branched nanoparticles to the biologically transparent NIR region for optimal PTT was further demonstrated. This was achieved through the introduction of Ag^+ as a shape-directing agent during the seeded growth process.^{22-24, 30-31} In the presence of gold seeds, Ag^+ is known to undergo reduction on gold surfaces at a potential less than the standard reduction potential of Ag^+/Ag^0 in a phenomenon known as ‘under-potential deposition’.^{24, 31-32} At low concentrations of added Ag^+ , the reduced Ag atoms have been found to preferentially deposit on the more open Au (110) facets thereby protecting them from further growth while promoting anisotropic growth of Au atoms on the (111) and (100) planes.³¹ As seen from Figure 2a, the introduction of Ag^+ enhanced the aspect ratio of the branches formed, giving rise to narrowly dispersed AuNUs capped with L-dopa and PEG on the surface. The mean diameter of the L-dopa functionalized AuNU core was found to be 83.9 ± 4.4 nm (Figure 2a insert), while tip-to-tip and spike lengths were found to be 121.1 ± 9.8 nm and 29.6 ± 7.6 nm, respectively (Table S2). A selected area (electron) diffraction (SAED) pattern characteristic of Au crystalline structures was observed from the AuNU branch (Figure 2b). With an increase in the aspect ratio of the branches, the L-dopa functionalized AuNUs were found to exhibit a broad plasmon spectrum, with a dominant longitudinal plasmon resonance peak at 808 nm and a weaker transverse peak at ~ 527 nm (Figure 2c). The presence of primary amine and carboxylic acid groups of the L-dopa molecules on the surface of the multi-branched AuNUs were confirmed using XPS analysis (Figure 2d and e). Control AuNUs were also synthesized using 4-ethylcatechol and were

found to have similar morphological and optical properties (Table S2 and Figure S6). As expected, XPS analysis confirmed the absence of both primary amine and carboxylic acid groups on the surface of the 4-ethylcatechol functionalized AuNUs (Figure 2d and e). The Au:Ag ratio on the surface of the AuNUs was determined from Au 4d and Ag 3d core levels to be 98:2 for both samples (Figure 2f).

A major limitation in the development of anisotropic AuNPs such as nanorods, nanoprisms, and nanostars for photothermal applications lies in the undesirable ageing phenomenon in which the AuNPs tend to rearrange into thermodynamically favorable spheres during long term storage or laser-induced heating,³³ resulting in the loss of original nanoparticle shape, aggregation of nanoparticles, and a resultant blue shift in the UV-vis absorption curve. This event has been attributed to the higher surface energy of gold atoms arising from the larger surface area in anisotropic AuNPs. In this study, we found that the catechol and PEG coating on the surface of the multi-branched AuNUs was able to effectively minimize the ageing process as seen from the unchanged UV-vis absorption spectrum over a period of 3 months (Figure S6b).

3.3. Cytotoxicity and LAT-1 targeted cellular uptake. The cytotoxicity of the functionalized AuNFs was first evaluated in the human breast cancer cell lines MCF-7 and MDA-MB-231 as well as the non-tumorigenic immortalized breast epithelial MCF-10A cell line. No overt cytotoxicity was induced by all the functionalized AuNFs of various sizes even at supraphysiological concentrations of up to 100 $\mu\text{g}/\text{mL}$ equivalent gold content in all three cell lines tested (Figure 3 and Figure S7). These results thus demonstrate that the functionalized AuNFs are biocompatible and are suitable for biomedical applications.

To evaluate the LAT-1 targeting efficiency, a panel of breast cancer cell lines including MCF-7, MDA-MB-231, MDA-MB-453, MDA-MB-468, and the non-tumorigenic MCF-10A cell line were incubated with the respective catechol-functionalized AuNFs and quantified for

intracellular gold content using ICP-AES. For each of the three sizes of AuNFs tested, it was observed that the L- and D-dopa functionalized AuNFs mediated significantly higher uptake in all four breast cancer cell lines when compared to the dopamine and 4-ethylcatechol functionalized AuNF controls ($P < 0.01$; Figure 4a-c). For instance, in the triple negative MDA-MB-231 cell line, it was found that approximately 17% of the added dose of both the 90 nm L-dopa and D-dopa functionalized AuNFs were taken up by the cells while $< 1\%$ of the dopamine and 4-ethylcatechol functionalized AuNFs were internalized (Figure 4b). The higher uptake of both the L- and D-dopa functionalized AuNFs in the breast cancer cell lines was consistent with reports on the ability of the LAT-1 to transport both the L and D isomers of bulky or branched amino acids in cancer cells.³⁴⁻³⁵ Notably, minimal uptake of L- and D-dopa functionalized AuNFs was observed in the non-tumorigenic MCF-10A cell line, hence demonstrating the selectivity of the L- and D-dopa functionalized AuNFs towards breast cancer cells (Figure 4d). It is also important to note that the LAT-1 targeting capabilities of the L- and D-dopa functionalized AuNFs appear to be preserved despite the possible surface adsorption of serum proteins on the nanoparticles as discussed in Section 3.1 (Figure S5).

To further investigate the mode of cellular uptake and intracellular distribution of the L-dopa and 4-ethylcatechol functionalized AuNFs, thin sections of treated MDA-MB-231 cells were prepared and imaged using HAADF-STEM. From Figure 5a and Figure S8, it can be observed that membrane invaginations occurred upon contact of the L-dopa functionalized AuNFs with the plasma membrane. The L-dopa functionalized AuNFs were predominantly found to be concentrated within vesicular structures, hence suggesting an endocytic mode of cellular uptake (Figure 5b and c). In contrast, very few of the non-targeting 4-ethylcatechol functionalized AuNFs were observed within the cells (Figure 5d). The endocytic mode of uptake for the L- and D-dopa functionalized AuNFs was further confirmed by the significant decrease in the amount of AuNFs internalized when the incubation temperature was reduced

from 37 °C to 4 °C ($P < 0.05$; Figure S9). In the literature, the clathrin-independent mode of endocytosis has been reported for the internalization of heterodimeric LAT-1-4F2hc complexes, which are taken into the cells via distinct vesicles that are subsequently transferred to early endosomes for sorting.³⁶⁻³⁷ It is believed that the mild acidic pH of the early endosomes then triggers conformational changes in the protein complex causing release of its cargo, hence enabling the transporter to be recycled back to the plasma membrane via tubular endosomes.

The role of LAT-1 in mediating uptake of the L-dopa functionalized AuNFs was investigated in a competition assay where the uptake of AuNFs by the MCF-7 breast cancer cells was determined in the presence of previously reported LAT-1 substrates phenylalanine (Phe) or serine (Ser).³⁴ In the presence of the high affinity substrate Phe ($K_m = 14.2 \mu\text{M}$), a dose-dependent decrease in the amount of L-dopa functionalized AuNFs internalized was observed, with uptake reduced to 84% and 70% of the control in the presence of 2 and 20 mM of Phe, respectively (Figure 6a; $P < 0.05$). The low affinity substrate Ser, on the other hand, did not induce significant decrease in the uptake of L-dopa functionalized AuNFs. As the concentrations of free amino acids and AuNFs used in this experiment did not induce overt cytotoxicity (Figure 3 and 6b), it is likely that the free Phe competed with the L-dopa functionalized AuNFs for interaction with the LAT-1, thereby leading to a reduction in nanoparticle uptake.

3.4. Effect of AuNP geometry on cellular uptake. As the size and shape of nanoparticles play an important role in influencing their biological properties,³⁸ we next evaluated the effect of particle size on the uptake of AuNFs using the MDA-MB-231 breast cancer cells. The nanoparticle concentration for a known gold content of each type of AuNF was first estimated using NTA (Table S1) and an approximately same number ($\sim 1.1 \times 10^{10}$ particles per well) of each of the AuNFs was incubated with the cells for 12 h. For each type of functionalization, a

size-dependent uptake of the AuNFs was found to occur in the following order: 90 nm > 70 nm > 46 nm ($P < 0.05$; Figure S10). For instance, an increase in the diameter of the L-dopa functionalized AuNFs from 46 to 70 and 90 nm, resulted in 3.0- and 3.7-fold increase in the number of particles taken up per cells, respectively. The influence of nanoparticle shape on the uptake of the AuNPs was further evaluated using the functionalized AuNFs and AuNUs with similar core diameters of approximately 90 and 84 nm, respectively (Figure 1d, 2a insert and Table S2). Whilst the cancer targeting properties of both the L-dopa functionalized AuNFs and AuNUs were preserved when compared to the 4-ethylcatechol functionalization, an increase in the aspect ratios of the nanoparticle branches from the flower-like to urchin-like morphology led to a slight decrease in cellular uptake at both concentrations tested ($P < 0.01$; Figure S11). This result is in agreement with previous studies in which spherical AuNPs or AuNPs having a shape closer to a sphere were found to promote greater cellular uptake when compared to star-shaped or urchin-like AuNPs in various cell types.³⁸

3.5. Photothermal properties of functionalized AuNUs. The photothermal properties of the L-dopa- and 4-ethylcatechol-functionalized AuNUs were investigated as a function of concentration during exposure to an 808 nm continuous wave laser at 3 W for 3 min. As shown in Figure 7a, laser irradiation of dispersions containing L-dopa functionalized AuNUs resulted in a gradual dose-dependent rise in temperature, with the highest temperature increase of 21 °C recorded at 50 µg/mL, while no significant temperature rise was observed with Milli-Q water. A similar heating profile was also obtained for the 4-ethylcatechol functionalized AuNUs, hence demonstrating that the type of coating did not affect the photothermal properties of the AuNUs (Figure S12). In addition, the laser irradiation of the L-dopa and 4-ethylcatechol functionalized AuNUs did not result in significant changes to the core diameter, tip-to-tip length, and the aspect ratio of the branched structures (Table S2). These results thus suggest that the coating of the multi-branched AuNUs with L-dopa or 4-

ethylcatechol and PEG was sufficient to maintain the structural stability of the AuNUs during photothermal heating and could potentially reduce the need for repeated nanoparticle dosing during the treatment course.

3.6. Selective photothermal ablation of breast cancer cells. In order to first simulate a situation whereby malignant breast cancer cells are exposed to photothermal agents in the interstitial fluids *in vivo*, L-dopa functionalized AuNUs were added to each well with cells adhered at the bottom and immediately subjected to NIR laser irradiation at 9.4 W/cm². Consistent with the thermal profiles observed earlier, the bulk heating of the extracellular medium resulted in a concentration-dependent decrease in MDA-MB-231 cell viability; with cell viability decreased to 75% at 5 µg/mL, and < 1% from 15 µg/mL and above (Figure 7b). To demonstrate targeted photothermal ablation of breast cancer cells by the L-dopa functionalized AuNUs, MDA-MB-231 cells were pre-treated with various concentrations of AuNUs for three days. Following pre-treatment, only a small amount of non-internalized L-dopa functionalized AuNUs was found to remain in the extracellular medium as compared to the 4-ethylcatechol functionalized AuNUs treated wells (Figure S13a). After rinsing the cells thoroughly to remove extracellular AuNUs, $\geq 80\%$ of the added dose of L-dopa functionalized AuNUs and $\leq 2\%$ of the 4-ethylcatechol functionalized AuNUs were found to be taken up by the cells (Figure S13b). Optical micrographs of the cells before and after laser irradiation were also recorded. Figure S14b and c shows the accumulation of dark L-dopa functionalized AuNUs granules within cells, while no nanoparticle clusters were visible in the untreated and 4-ethylcatechol functionalized AuNUs treated cells (Figure S14a, d, and e). Immediately after laser irradiation, the cells that have internalized L-dopa functionalized AuNUs appeared rounded up whereas minimal or no changes in cell morphology were observed for the untreated cells and cells treated with 4-ethylcatechol functionalized AuNUs (right panels of Figure S14b and c vs. Figure S14a, d, and e). An evaluation of the cell

viability 24 h after laser irradiation showed that cells that have been pre-treated with 50 and 100 $\mu\text{g/mL}$ L-dopa functionalized AuNUs had significantly reduced cell viability of 30% and 16%, respectively (Figure 7c). In contrast, cells treated with the non-targeting 4-ethylcatechol functionalized AuNUs were fully viable at the same irradiation dosage (Figure 7d), hence clearly demonstrating the ability of the L-dopa functionalized AuNUs to mediate selective photothermal ablation of breast cancer cells. In the absence of laser exposure, cells that were separately treated with L-dopa- and 4-ethylcatechol-functionalized AuNUs were not found to be toxic at the dosages tested. The selective PTT mediated by the L-dopa functionalized AuNUs could be further demonstrated by the confined detachment of non-viable cells 24 h after laser irradiation, giving rise to a relatively empty zone within the laser spot (outlined by white dotted line), while cells outside the zone of laser irradiation remained largely viable (Figure 7e). On the other hand, the cell monolayer treated with the non-targeting 4-ethylcatechol functionalized AuNUs remained fully intact and viable after laser treatment as evidenced from the uniform green fluorescent staining of live cells by the cell permeant calcein AM dye as well as absence of red fluorescent staining of non-viable cells by the ethidium homodimer-1 dye (Figure 7f). These results thus demonstrate that the localized laser irradiation of cells that have internalized the LAT-1 targeting AuNUs serves as a secondary form of targeting to overcome unwanted side effects frequently observed with traditional chemotherapy and hyperthermia therapy. As a proof-of-concept for the use of L-dopa functionalized AuNU-mediated PTT to sensitize cancer cells to conventional chemotherapy, the pre-treated MDA-MB-231 breast cancer cells were first subjected to laser irradiation and subsequently exposed to cisplatin (Cis) and docetaxel (DTX), which are first-line chemotherapeutic agents used in the clinical treatment of TNBC. At the highest dose of L-dopa functionalized AuNU used for pre-treatment, the cells demonstrated a cell viability of 16% when subjected to PTT alone (Figure 8). Cells treated with Cis alone had cell viability of

61%. The combination of PTT and Cis led to a significant reduction in cell viability to 4% ($P < 0.05$), which was less than the 9.8% cell viability expected if the combination effect was additive, hence suggesting synergistic effects.³⁹ Similarly, treatment of the cells with DTX alone resulted in a cell viability of 84%. The combination of PTT and DTX at the 100 $\mu\text{g}/\text{mL}$ pre-treatment dose of L-dopa functionalized AuNUs used led to a significant reduction in cell viability to 1% ($P < 0.01$), which was again lower than the 13.4% cell viability expected in the case of additive effects. These results were thus consistent with previous reports in which PTT was found to increase membrane permeability thereby leading to enhanced drug accumulation and cytotoxicity in cancer cells.^{4,39}

4. Conclusions

In this study, a simple and versatile method was developed for the synthesis of multi-branched AuNPs with active cancer targeting capabilities via the LAT-1. By utilizing catechol-containing LAT-1 ligands in the seed mediated reduction of gold ions, monodispersed nanoflower-like AuNPs with excellent stability, biocompatibility, and targeting to a panel of breast cancer cell lines even in the presence of serum-containing media were obtained. The direct synthesis of cancer targeting multi-branched AuNPs using LAT-1 ligands circumvents the need for cytotoxic surfactants as well as additional conjugation procedures, hence potentially offering time and cost savings for the large scale production of biofriendly AuNPs. Additionally, the introduction of silver ions during synthesis gave rise to sea urchin-like AuNPs (AuNUs) with strong absorbance in the NIR window, which enabled them to be used in the selective photothermal ablation of the triple negative MDA-MB-231 breast cancer line. In addition, the PTT mediated by the L-dopa functionalized AuNUs sensitized breast cancer cells to the cytotoxic effects of conventional chemotherapeutic agents cisplatin and docetaxel. Taken together, the cancer targeting L- or D-dopa functionalized

AuNUs may have potential to be used for the *in vivo* targeted photothermal ablation of breast cancers, especially against the triple negative subtype, for which there is currently no targeted therapy. As LAT-1 is frequently overexpressed in numerous proliferating tumors, this technology may also have broad applications for the PTT of other cancer types.

ASSOCIATED CONTENT

Supporting Information. Additional information on the physicochemical properties, XPS characterization, colloidal stability, cytotoxicity, thermal profiles, and cellular uptake of the synthesized AuNPs are provided. The Supporting Information is available free of charge on the ACS Publications website.

AUTHOR INFORMATION

Corresponding Author

*E-mail: z.y.ong@leeds.ac.uk (Z.Y.O.)

Present Addresses

†If an author's address is different than the one given in the affiliation line, this information may be included here.

Author Contributions

The manuscript was written through contributions of all authors. All authors have given approval to the final version of the manuscript.

ACKNOWLEDGMENT

This work was supported by the People Programme (Marie Curie Actions) of the European Union's Seventh Framework Programme FP7-PEOPLE-2013-IIF under REA grant agreement n° [624475] (Z.Y.O.) and an ERC starting grant to AEP (CNTBBB).

REFERENCES

1. WHO Breast cancer: prevention and control. <http://www.who.int/cancer/detection/breastcancer/en/> (accessed 22 July 2017).
2. Bianchini, G.; Balko, J. M.; Mayer, I. A.; Sanders, M. E.; Gianni, L., Triple-negative breast cancer: challenges and opportunities of a heterogeneous disease. *Nat. Rev. Clin. Oncol.* **2016**, *13* (11), 674.
3. Li, N.; Zhao, P.; Astruc, D., Anisotropic gold nanoparticles: synthesis, properties, applications, and toxicity. *Angew. Chem., Int. Ed.* **2014**, *53* (7), 1756-1789.
4. Abadeer, N. S.; Murphy, C. J., Recent progress in cancer thermal therapy using gold nanoparticles. *J. Phys. Chem. C* **2016**, *120* (9), 4691-4716.
5. Huang, X.; El-Sayed, M. A., Gold nanoparticles: optical properties and implementations in cancer diagnosis and photothermal therapy. *J. Adv. Res.* **2010**, *1* (1), 13-28.
6. Chen, F.; Cai, W., Nanomedicine for targeted photothermal cancer therapy: where are we now? *Nanomedicine* **2015**, *10* (1), 1-3.
7. Stern, J. M.; Kibanov Solomonov, V. V.; Sazykina, E.; Schwartz, J. A.; Gad, S. C.; Goodrich, G. P., Initial evaluation of the safety of nanoshell-directed photothermal therapy in the treatment of prostate disease. *Int. J. Toxicol.* **2016**, *35* (1), 38-46.
8. Li, J.; Hu, Y.; Yang, J.; Wei, P.; Sun, W.; Shen, M.; Zhang, G.; Shi, X., Hyaluronic acid-modified Fe₃O₄@Au core/shell nanostars for multimodal imaging and photothermal therapy of tumors. *Biomaterials* **2015**, *38*, 10-21.
9. Uchino, H.; Kanai, Y.; Kim, D. K.; Wempe, M. F.; Chairoungdua, A.; Morimoto, E.; Anders, M.; Endou, H., Transport of amino acid-related compounds mediated by L-type amino acid transporter 1 (LAT1): insights into the mechanisms of substrate recognition. *Mol. Pharmacol.* **2002**, *61* (4), 729-737.
10. Wang, Q.; Holst, J., L-type amino acid transport and cancer: targeting the mTORC1 pathway to inhibit neoplasia. *Am. J. Cancer Res.* **2015**, *5* (4), 1281.
11. Liang, Z.; Cho, H. T.; Williams, L.; Zhu, A.; Liang, K.; Huang, K.; Wu, H.; Jiang, C.; Hong, S.; Crowe, R., Potential biomarker of L-type amino acid transporter 1 in breast cancer progression. *Nucl. Med. Mol. Imaging* **2011**, *45* (2), 93-102.
12. Furuya, M.; Horiguchi, J.; Nakajima, H.; Kanai, Y.; Oyama, T., Correlation of L - type amino acid transporter 1 and CD98 expression with triple negative breast cancer prognosis. *Cancer Sci.* **2012**, *103* (2), 382-389.
13. Shennan, D. B.; Thomson, J., Inhibition of system L (LAT1/CD98hc) reduces the growth of cultured human breast cancer cells. *Oncol. Rep.* **2008**, *20* (4), 885-889.
14. Li, L.; Di, X.; Wu, M.; Sun, Z.; Zhong, L.; Wang, Y.; Fu, Q.; Kan, Q.; Sun, J.; He, Z., Targeting tumor highly-expressed LAT1 transporter with amino acid-modified nanoparticles: Toward a novel active targeting strategy in breast cancer therapy. *Nanomedicine (N. Y., NY, U. S.)* **2017**, *13* (3), 987-998.

15. Li, L.; Di, X.; Zhang, S.; Kan, Q.; Liu, H.; Lu, T.; Wang, Y.; Fu, Q.; Sun, J.; He, Z., Large amino acid transporter 1 mediated glutamate modified docetaxel-loaded liposomes for glioma targeting. *Colloids and Surfaces B: Biointerfaces* **2016**, *141*, 260-267.
16. Baron, R.; Zayats, M.; Willner, I., Dopamine-, L-DOPA-, adrenaline-, and noradrenaline-induced growth of Au nanoparticles: assays for the detection of neurotransmitters and of tyrosinase activity. *Anal. Chem.* **2005**, *77* (6), 1566-1571.
17. Lu, C. C.; Zhang, M.; Li, A. J.; He, X. W.; Yin, X. B., 3, 4 - Dihydroxy - L - phenylalanine for Preparation of Gold Nanoparticles and as Electron Transfer Promoter in H₂O₂ Biosensor. *Electroanalysis* **2011**, *23* (10), 2421-2428.
18. Gachard, E.; Remita, H.; Khatouri, J.; Keita, B.; Nadjo, L.; Belloni, J., Radiation-induced and chemical formation of gold clusters. *New J. Chem.* **1998**, *22* (11), 1257-1265.
19. Perrault, S. D.; Chan, W. C., Synthesis and surface modification of highly monodispersed, spherical gold nanoparticles of 50– 200 nm. *J. Am. Chem. Soc.* **2009**, *131* (47), 17042-17043.
20. Li, J.; Wang, W.; Zhao, L.; Rong, L.; Lan, S.; Sun, H.; Zhang, H.; Yang, B., Hydroquinone-assisted synthesis of branched Au–Ag nanoparticles with polydopamine coating as highly efficient photothermal agents. *ACS Appl. Mater. Interfaces* **2015**, *7* (21), 11613-11623.
21. Li, J.; Wu, J.; Zhang, X.; Liu, Y.; Zhou, D.; Sun, H.; Zhang, H.; Yang, B., Controllable synthesis of stable urchin-like gold nanoparticles using hydroquinone to tune the reactivity of gold chloride. *J. Phys. Chem. C* **2011**, *115* (9), 3630-3637.
22. Cheng, L.-C.; Huang, J.-H.; Chen, H. M.; Lai, T.-C.; Yang, K.-Y.; Liu, R.-S.; Hsiao, M.; Chen, C.-H.; Her, L.-J.; Tsai, D. P., Seedless, silver-induced synthesis of star-shaped gold/silver bimetallic nanoparticles as high efficiency photothermal therapy reagent. *J. Mater. Chem.* **2012**, *22* (5), 2244-2253.
23. Yuan, H.; Ma, W.; Chen, C.; Zhao, J.; Liu, J.; Zhu, H.; Gao, X., Shape and SPR evolution of thorny gold nanoparticles promoted by silver ions. *Chem. Mater.* **2007**, *19* (7), 1592-1600.
24. Personick, M. L.; Langille, M. R.; Zhang, J.; Mirkin, C. A., Shape control of gold nanoparticles by silver underpotential deposition. *Nano Lett.* **2011**, *11* (8), 3394-3398.
25. McGrath, A. J.; Chien, Y.-H.; Cheong, S.; Herman, D. A.; Watt, J.; Henning, A. M.; Gloag, L.; Yeh, C.-S.; Tilley, R. D., Gold over branched palladium nanostructures for photothermal cancer therapy. *ACS nano* **2015**, *9* (12), 12283-12291.
26. Yuan, H.; Fales, A. M.; Vo-Dinh, T., TAT peptide-functionalized gold nanostars: enhanced intracellular delivery and efficient NIR photothermal therapy using ultralow irradiance. *J. Am. Chem. Soc.* **2012**, *134* (28), 11358-11361.
27. Gentry, S. T.; Fredericks, S. J.; Krchnavek, R., Controlled particle growth of silver sols through the use of hydroquinone as a selective reducing agent. *Langmuir* **2009**, *25* (5), 2613-2621.
28. Huang, D.; Zhou, H.; Liu, H.; Gao, J., The cytotoxicity of gold nanoparticles is dispersity-dependent. *Dalton Trans.* **2015**, *44* (41), 17911-17915.
29. Wong-Ng, W.; McMurdie, H.; Hubbard, C.; Mighell, A. D., JCPDS-ICDD research associateship (cooperative program with NBS/NIST). *J. Res. Natl. Inst. Stand. Technol.* **2001**, *106* (6), 1013.
30. Ahmed, W.; Kooij, E. S.; Van Silfhout, A.; Poelsema, B., Controlling the morphology of multi-branched gold nanoparticles. *Nanotechnology* **2010**, *21* (12), 125605.
31. Liu, M.; Guyot-Sionnest, P., Mechanism of silver (I)-assisted growth of gold nanorods and bipyramids. *J. Phys. Chem. B* **2005**, *109* (47), 22192-22200.

32. Herrero, E.; Buller, L. J.; Abruña, H. D., Underpotential deposition at single crystal surfaces of Au, Pt, Ag and other materials. *Chem. Rev.* **2001**, *101* (7), 1897-1930.
33. González-Rubio, G.; Guerrero-Martínez, A.; Liz-Marzán, L. M., Reshaping, Fragmentation, and Assembly of Gold Nanoparticles Assisted by Pulse Lasers. *Acc. Chem. Res.* **2016**, *49* (4), 678-686.
34. Yanagida, O.; Kanai, Y.; Chairoungdua, A.; Kim, D. K.; Segawa, H.; Nii, T.; Cha, S. H.; Matsuo, H.; Fukushima, J.-i.; Fukasawa, Y., Human L-type amino acid transporter 1 (LAT1): characterization of function and expression in tumor cell lines. *Biochim. Biophys. Acta, Biomembr.* **2001**, *1514* (2), 291-302.
35. Shennan, D. B.; Thomson, J.; Gow, I. F.; Travers, M.; Barber, M., L-leucine transport in human breast cancer cells (MCF-7 and MDA-MB-231): kinetics, regulation by estrogen and molecular identity of the transporter. *Biochim. Biophys. Acta, Biomembr.* **2004**, *1664* (2), 206-216.
36. Grant, B. D.; Donaldson, J. G., Pathways and mechanisms of endocytic recycling. *Nat. Rev. Mol. Cell Biol.* **2009**, *10* (9), 597.
37. Maldonado-Báez, L.; Williamson, C.; Donaldson, J. G., Clathrin-independent endocytosis: a cargo-centric view. *Exp. Cell Res.* **2013**, *319* (18), 2759-2769.
38. Dykman, L. A.; Khlebtsov, N. G., Uptake of engineered gold nanoparticles into mammalian cells. *Chem. Rev.* **2013**, *114* (2), 1258-1288.
39. Fay, B. L.; Melamed, J. R.; Day, E. S., Nanoshell-mediated photothermal therapy can enhance chemotherapy in inflammatory breast cancer cells. *Int. J. Nanomed.* **2015**, *10*, 6931.

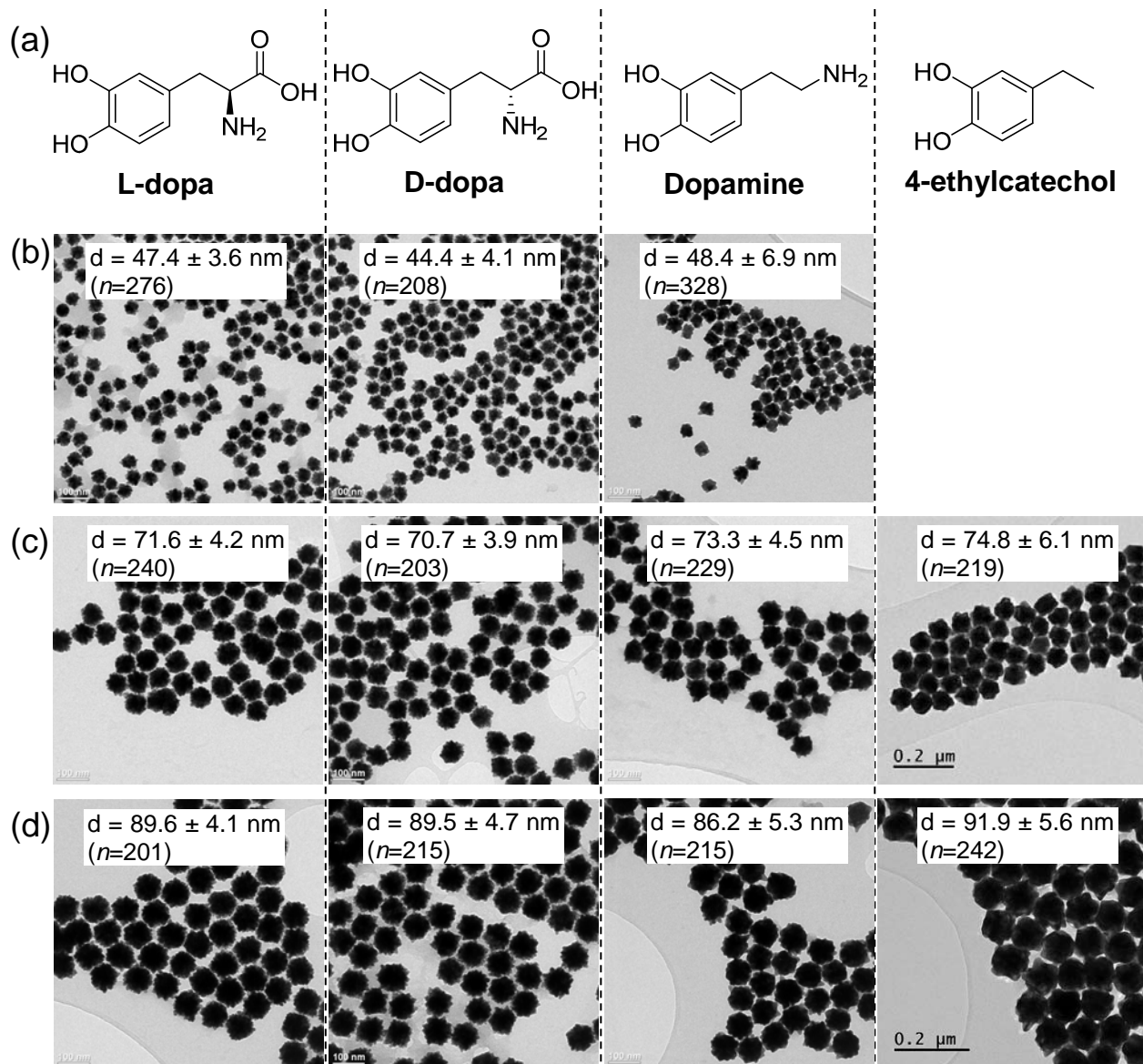


Figure 1. (a) Catechols employed in the synthesis and functionalization of multi-branched AuNPs in this study. (b-d) TEM images of catechol-functionalized AuNFs that were prepared using (b) 12.5, (c) 50, and (d) 100 μL of 0.1M $\text{HAuCl}_4 \cdot 3\text{H}_2\text{O}$. Particle size distribution was determined from the obtained TEM images using the ImageJ software.

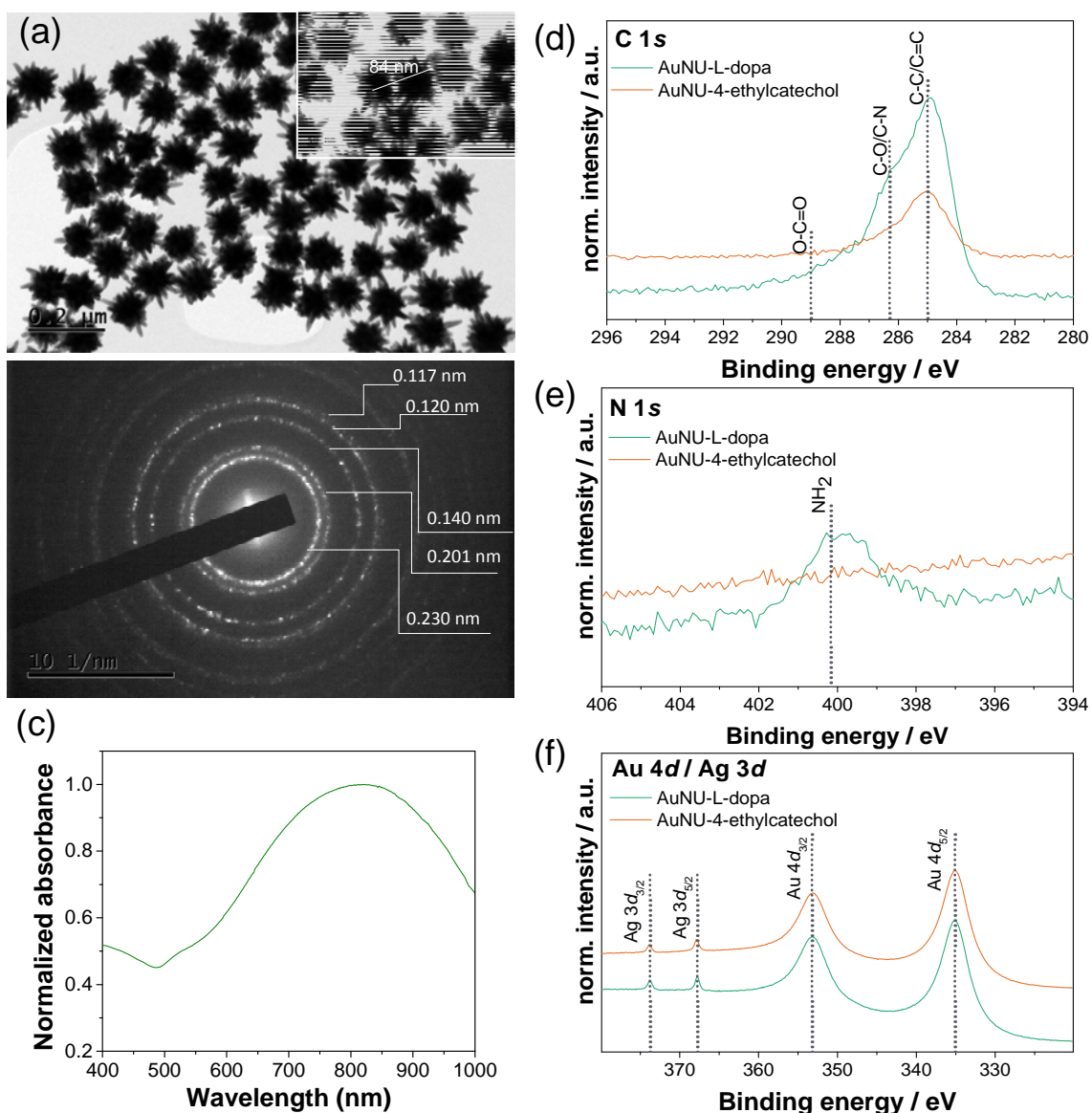


Figure 2. Representative (a) TEM image with core measurement (insert), (b) selected area electron diffraction (SAED) pattern, and (c) UV-vis absorbance spectrum of L-dopa functionalized AuNUs with LSPR peak absorbance tuned towards the NIR region. X-ray photoelectron spectroscopy (XPS) spectra obtained for L-dopa and 4-ethylcatechol functionalized AuNUs indicating (d) C 1s, (e) N, and (f) Au 4d and Ag 3d core levels.

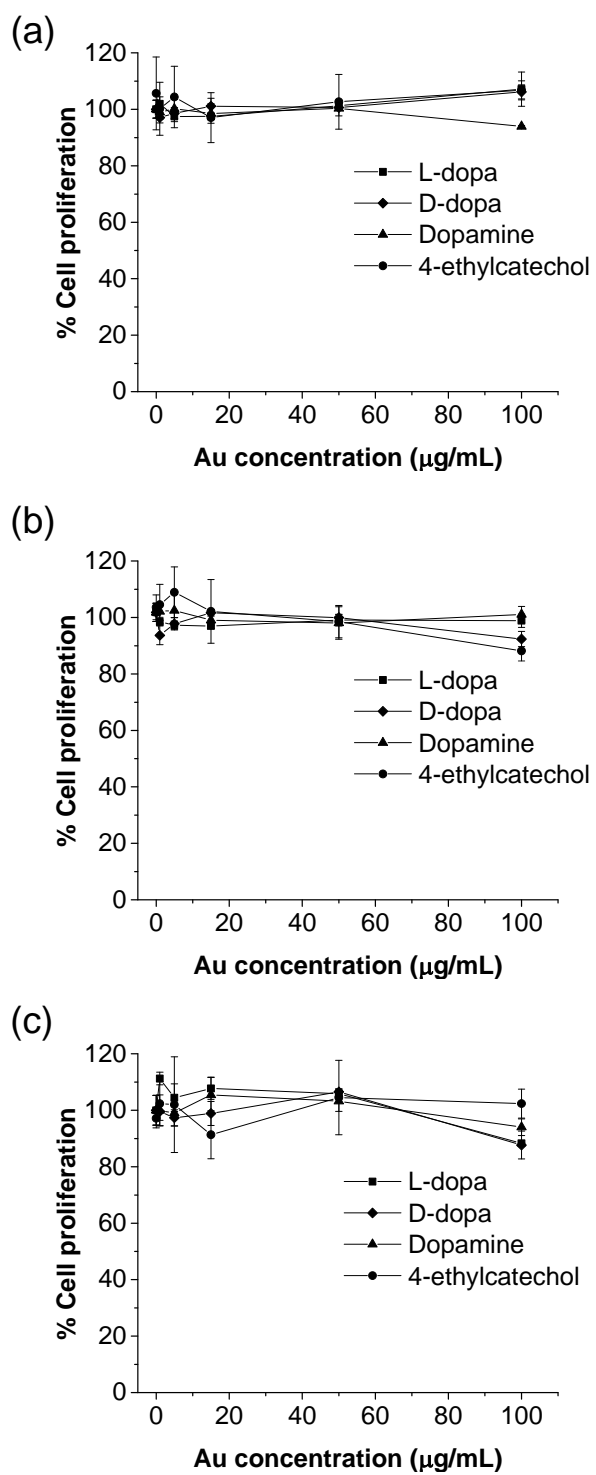


Figure 3. Effect of 90 nm catechol-functionalized AuNFs treatment on cell proliferation in (a) MCF-7, (b) MDA-MB-231, and (c) MCF-10A determined using WST-1 assay.

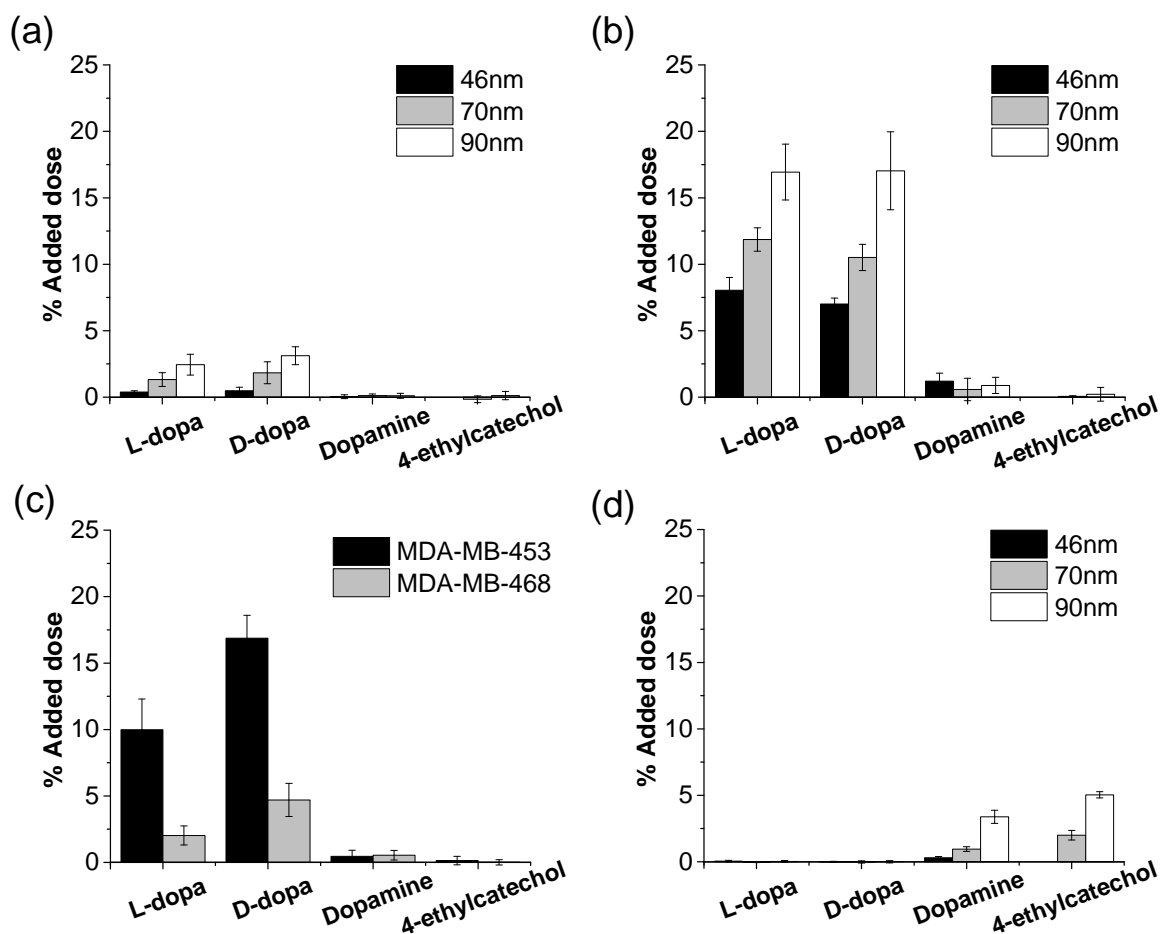


Figure 4. Uptake of catechol-functionalized AuNFs by breast cancer cell lines (a) MCF-7, (b) MDA-MB-231, (c) MDA-MB-453 and MDA-MB-468 (90 nm), and (d) non-tumorigenic MCF-10A treated with 15 $\mu\text{g}/\text{mL}$ of AuNFs for 12 h determined using ICP-AES. Results represent mean \pm standard deviation from at least two independent experiments performed in triplicates.

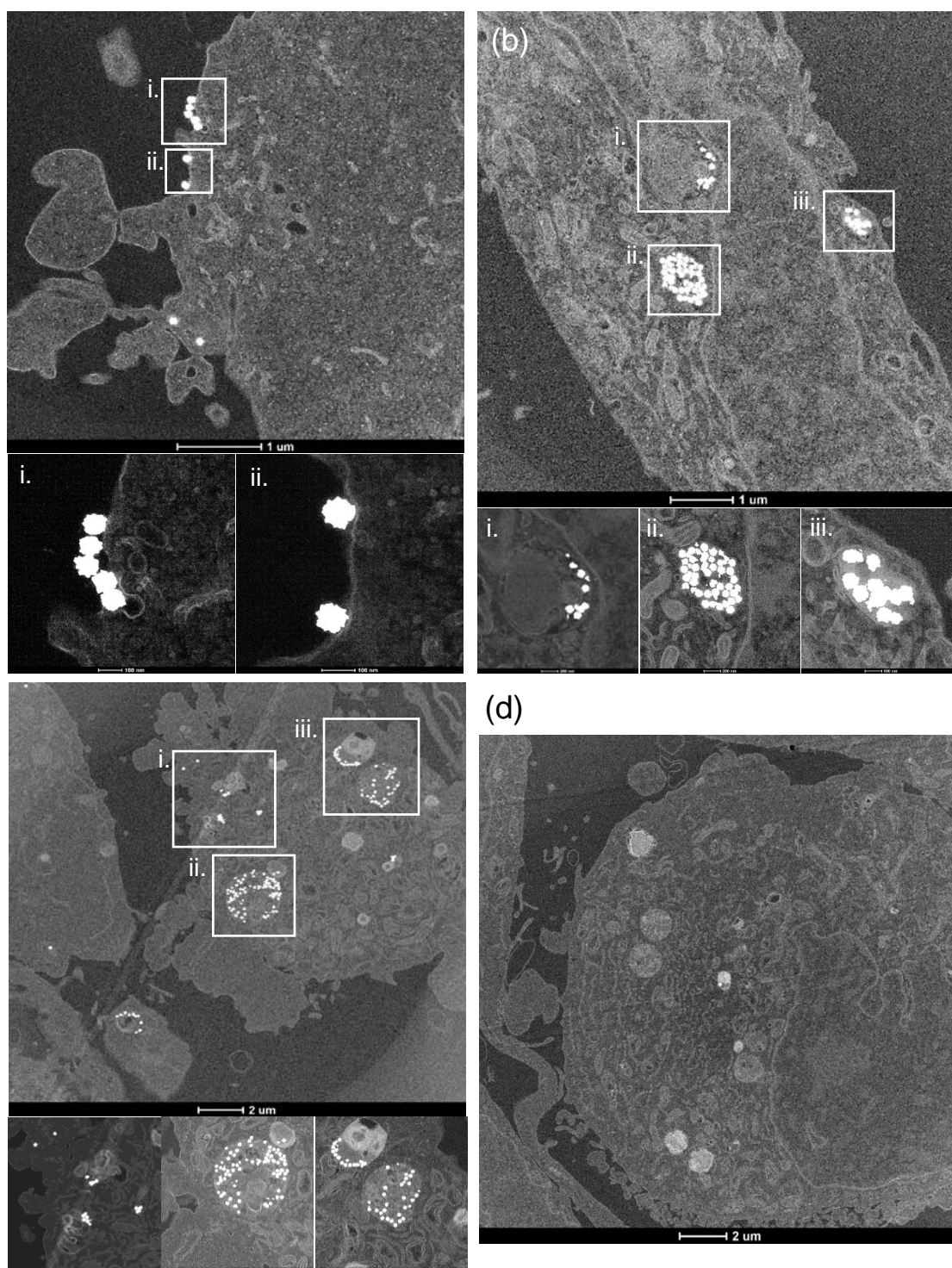


Figure 5. HAADF-STEM images of MDA-MB-231 after incubation with 90 nm L-dopa- and 4-ethylcatechol-functionalized AuNFs. (a) Cellular uptake of L-dopa functionalized AuNFs and (b) accumulation of L-dopa functionalized AuNFs inside vesicles after 4 h treatment. (c) Similar distribution of L-dopa functionalized AuNFs in vesicles was observed after 12 h treatment. (d) Representative cell section showing minimal or no 4-ethylcatechol functionalized AuNF uptake even after 12 h treatment.

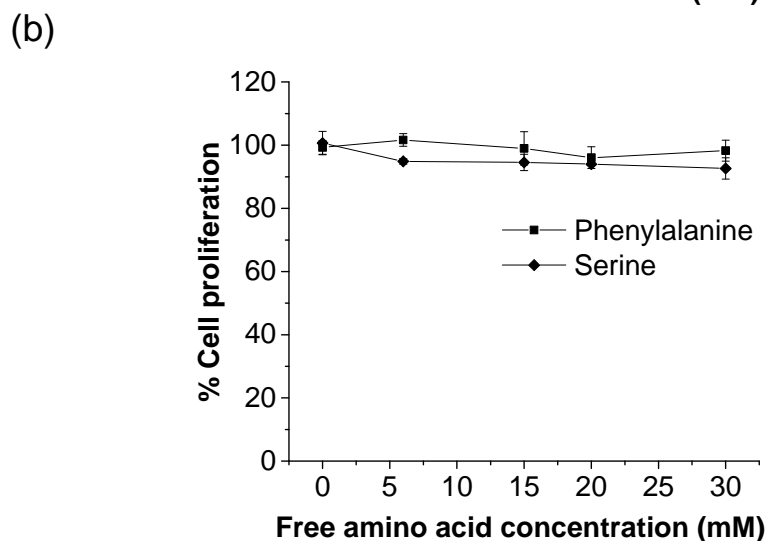
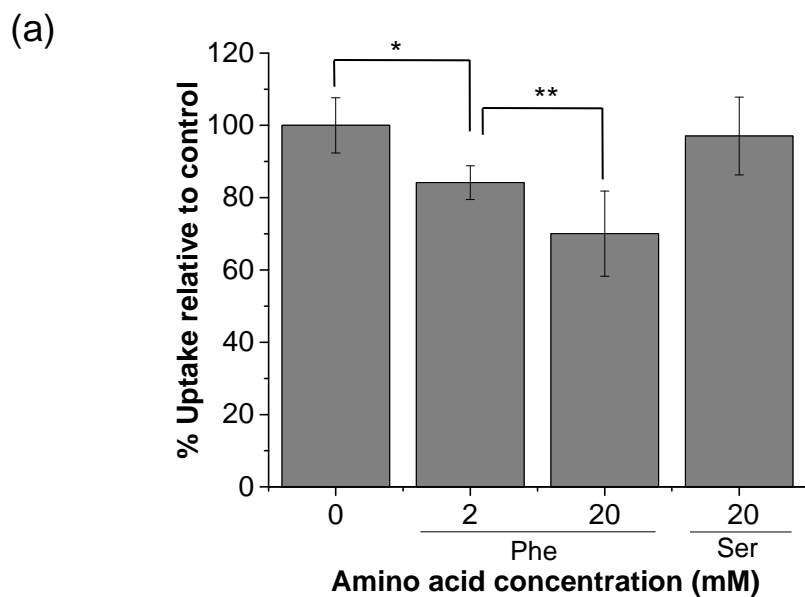


Figure 6. (a) Competitive inhibition of L-dopa functionalized AuNF uptake in MCF-7 in the presence of free LAT-1 ligands following 5 h incubation (* $P < 0.01$; ** $P < 0.05$). Results represent mean \pm standard deviation from three independent experiments performed in triplicates. (b) Cell viability of MCF-7 following free amino acid treatment for 5 h.

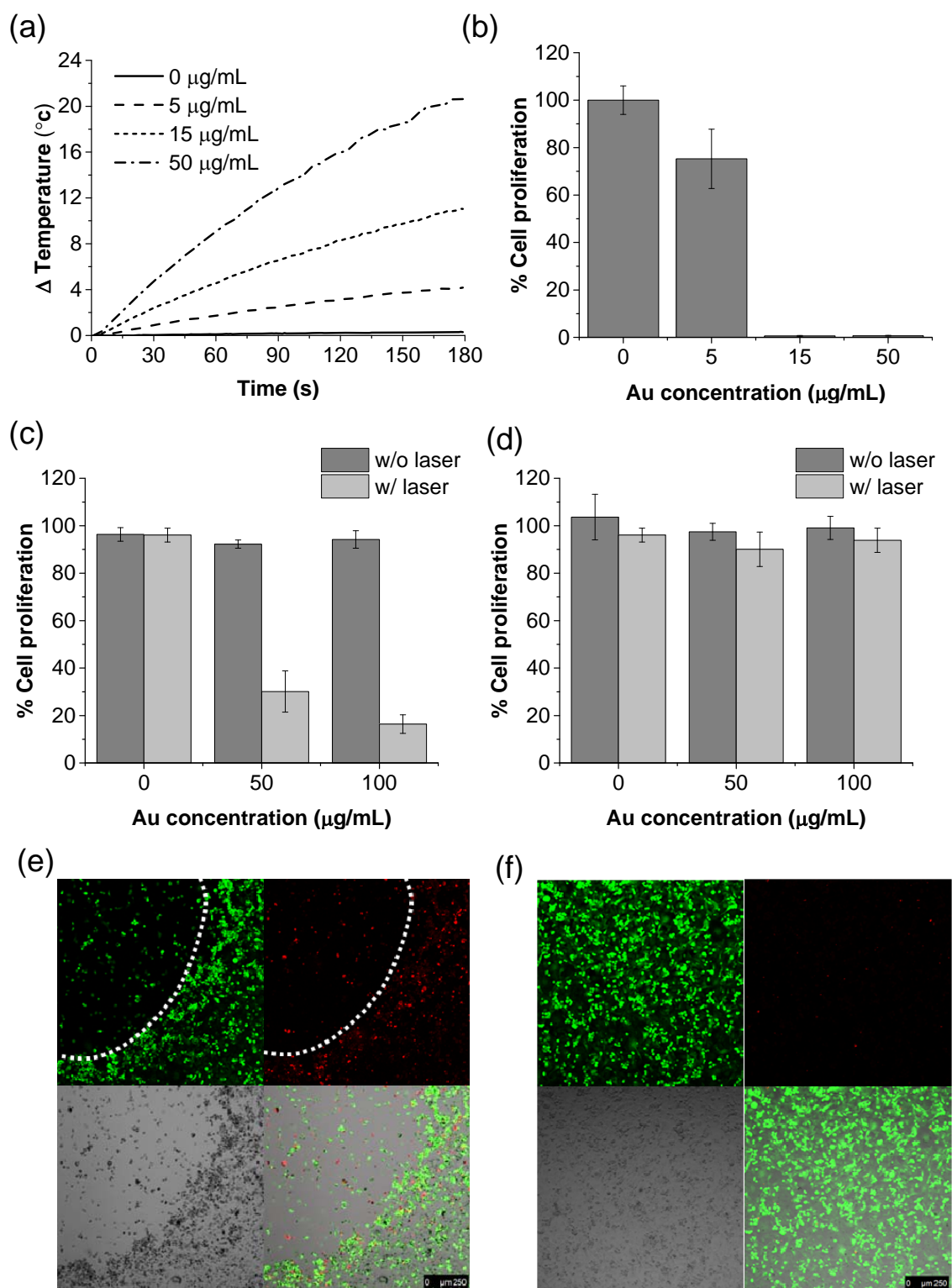


Figure 7. Photothermal effects of functionalized AuNUs following laser treatment. (a) Heating curve of L-dopa functionalized AuNUs following irradiation with 808 nm laser at 9.4 W/cm². (b) Cell viability of triple negative MDA-MB-231 breast cancer cell line exposed to increasing concentrations of extracellular L-dopa functionalized AuNUs added just before laser irradiation. Cell viability of MDA-MB-231 cells that have internalized (c) L-dopa functionalized AuNUs and (d) 4-ethylcatechol functionalized AuNUs with (w/) and without (w/o) laser exposure. Confocal scanning laser microscopy images after laser irradiation of

MDA-MB-231 that have internalized (e) L-dopa functionalized AuNUs and (f) 4-ethylcatechol functionalized AuNUs. Live cells are stained green while dead cells appear red.

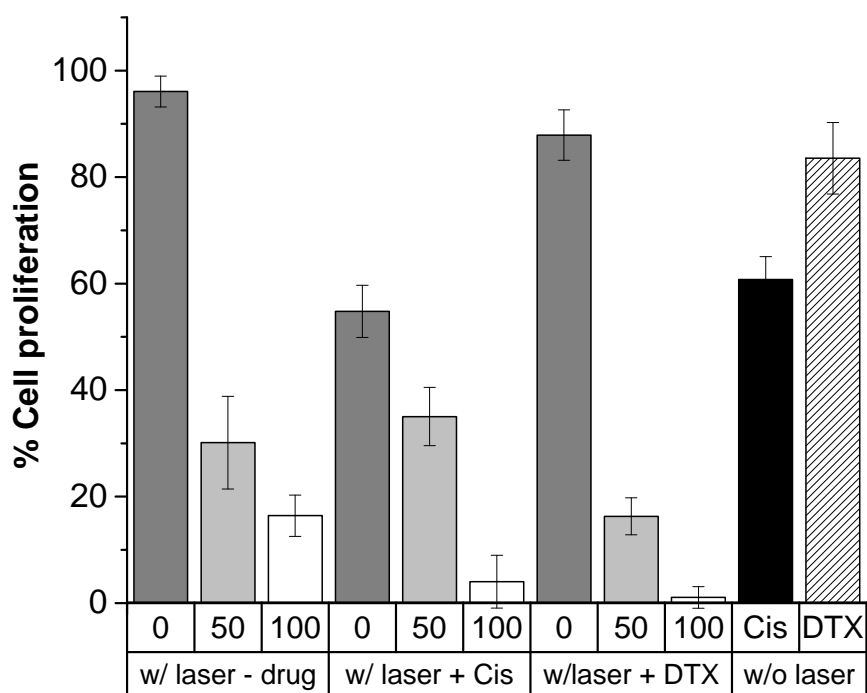
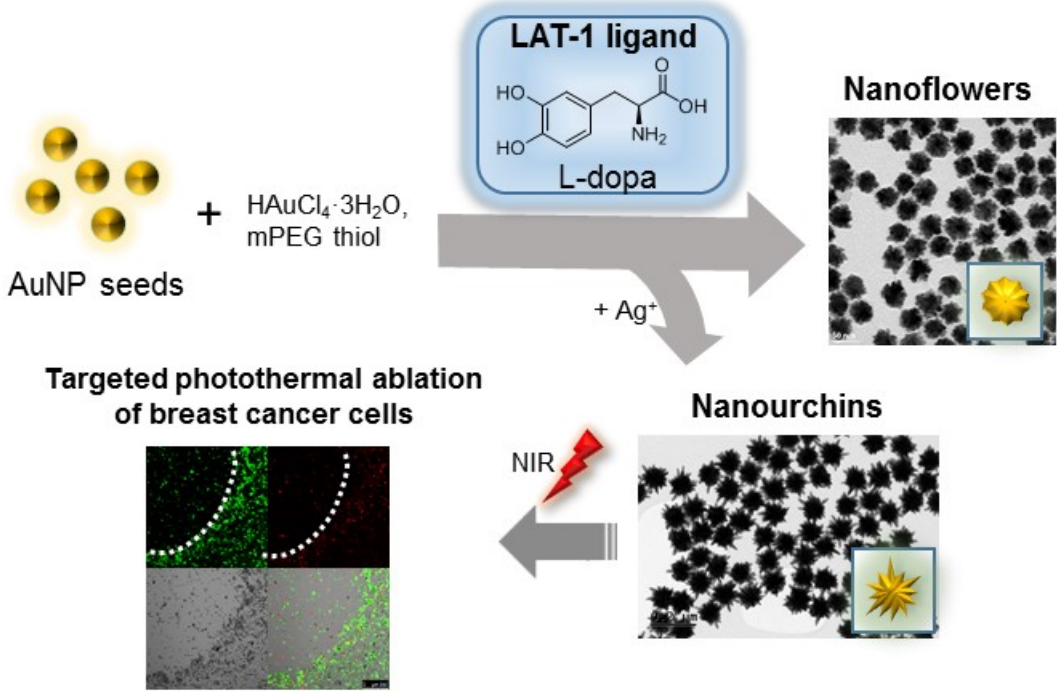


Figure 8. Sensitization of MDA-MB-231 cells to 83 μ M cisplatin (Cis) and 100 nM docetaxel (DTX) following laser irradiation of cells pre-treated with L-dopa functionalized AuNUs at the indicated concentrations (in μ g/mL).

Graphical abstract



Supporting Information

Multi-Branched Gold Nanoparticles with Intrinsic LAT-1 Targeting Capabilities for Selective Photothermal Therapy of Breast Cancer

Zhan Yuin Ong, Shu Chen, Elham Nabavi, Anna Regoutz, Alexandra Porter, Iain Dunlop, David Dexter and Daniel Elson*

Stability testing: 90 nm L-dopa functionalized AuNFs were dispersed in 800 μ L of deionized water, 1 \times PBS (pH 7.4), MEM cell culture medium with 10% fetal bovine serum, and 100% FBS at a concentration of 30 μ g/mL equivalent Au content, and incubated at 37 $^{\circ}$ C on an orbital shaker (600 rpm) to mimic blood circulation. At 0, 4, 24, 48, and 72 h, the hydrodynamic size and polydispersity of the samples were monitored by dynamic light scattering.

Size-dependent uptake of AuNFs: MDA-MB-231 cells were seeded onto 12-well plates at a density of 2.5×10^5 cells per well and allowed to adhere overnight. The incubation media in each well was replaced with cell culture media containing approximately 1.1×10^{10} of each type of AuNFs. After 12 h incubation at 37 $^{\circ}$ C, non-internalized AuNFs were removed, and the cells were rinsed thoroughly with 1 mL of PBS for 5 times. The cells were then trypsinized, rinsed once with PBS, and pelleted by centrifugation at 1300 \times rpm for 4 min. Trypan blue staining was performed to determine the number of viable cells in each sample. The Au content was analyzed by ICP-MS following aqua regia digestion. The number of particles internalized per sample was subsequently converted from the Au content obtained and normalized by the number of viable cells in each sample.

Table S1. Particle size, zeta-potential, and polydispersity index (PDI) of synthesized AuNFs

Designation	AuNP functionalization	Diameter \pm S.D. (nm) ^a	Z-average diameter \pm S.D. (nm) ^b	PDI ^b	Zeta-potential \pm S.D. (mV) ^b	Concentration (particles/mL) ^c
46 nm	L-dopa	47.4 \pm 3.6	62.9 \pm 0.7	0.17	-39.4 \pm 1.2	7.02 \times 10 ⁸
	D-dopa	44.4 \pm 4.1	62.6 \pm 0.1	0.22	-37.4 \pm 0.7	7.30 \times 10 ⁸
	Dopamine	48.4 \pm 6.9	55.5 \pm 0.1	0.24	-36.5 \pm 1.3	7.23 \times 10 ⁸
70 nm	L-dopa	71.6 \pm 4.2	89.8 \pm 0.6	0.05	-41.0 \pm 1.5	2.82 \times 10 ⁸
	D-dopa	70.7 \pm 3.9	96.9 \pm 0.7	0.15	-36.3 \pm 0.4	2.99 \times 10 ⁸
	Dopamine	73.3 \pm 4.5	89.3 \pm 0.5	0.07	-32.9 \pm 0.1	3.11 \times 10 ⁸
	4-ethylcatechol	74.8 \pm 6.1	88.9 \pm 0.8	0.09	-35.1 \pm 0.7	3.19 \times 10 ⁸
90 nm	L-dopa	89.6 \pm 4.1	116.5 \pm 0.7	0.02	-34.6 \pm 1.0	1.84 \times 10 ⁸
	D-dopa	89.5 \pm 4.7	112.6 \pm 0.8	0.04	-37.5 \pm 0.4	1.80 \times 10 ⁸
	Dopamine	86.2 \pm 5.3	111.2 \pm 1.1	0.02	-32.6 \pm 0.2	1.67 \times 10 ⁸
	4-ethylcatechol	91.9 \pm 5.6	108.3 \pm 0.1	0.04	-35.3 \pm 0.9	1.87 \times 10 ⁸

^a)By TEM measurement; ^b)By dynamic light scattering; ^c)Particle concentration of 1 μ g/mL Au equivalent dispersion determined using NanoSight NTA concentration measurement upgrade.

Table S2. Quantitative analysis of Ag/AuNP-L-dopa and Ag/AuNP-4-ethylcatechol with and without laser exposure using TEM images by ImageJ software.

Laser irradiation	Ag/AuNP type	Core diameter (nm)	Tip-to-tip length (nm)	Spike length (nm)	Aspect ratio
Before	L-dopa	83.9 ± 4.4 (n=110)	121.1 ± 9.8 (n=86)	29.6 ± 7.6 (n=58)	2.2 ± 0.6 (n=58)
	4-ethylcatechol	83.7 ± 5.7 (n=194)	112.3 ± 9.4 (n=187)	29.5 ± 8.2 (n=101)	1.6 ± 0.4 (n=101)
After	L-dopa	85.5 ± 7.0 (n=38)	124.1 ± 9.0 (n=38)	32.5 ± 7.9 (n=34)	2.2 ± 0.6 (n=34)
	4-ethylcatechol	84.9 ± 6.2 (n=133)	122.3 ± 10.1 (n=112)	33.1 ± 8.1 (n=116)	1.9 ± 0.5 (n=116)

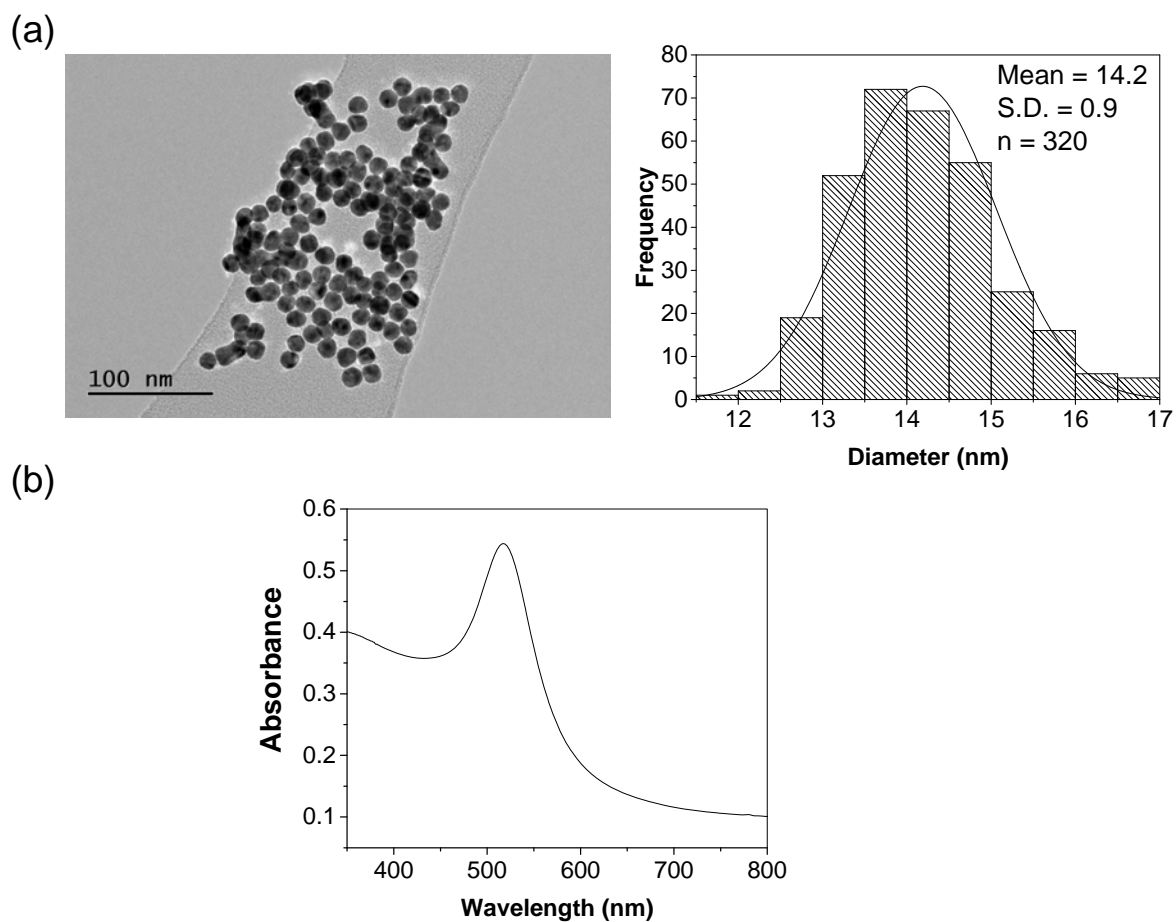


Figure S1. (a) TEM image with size distribution, and (b) UV-vis absorption spectrum of spherical citrate-capped gold seeds synthesized using the Turkevich method.

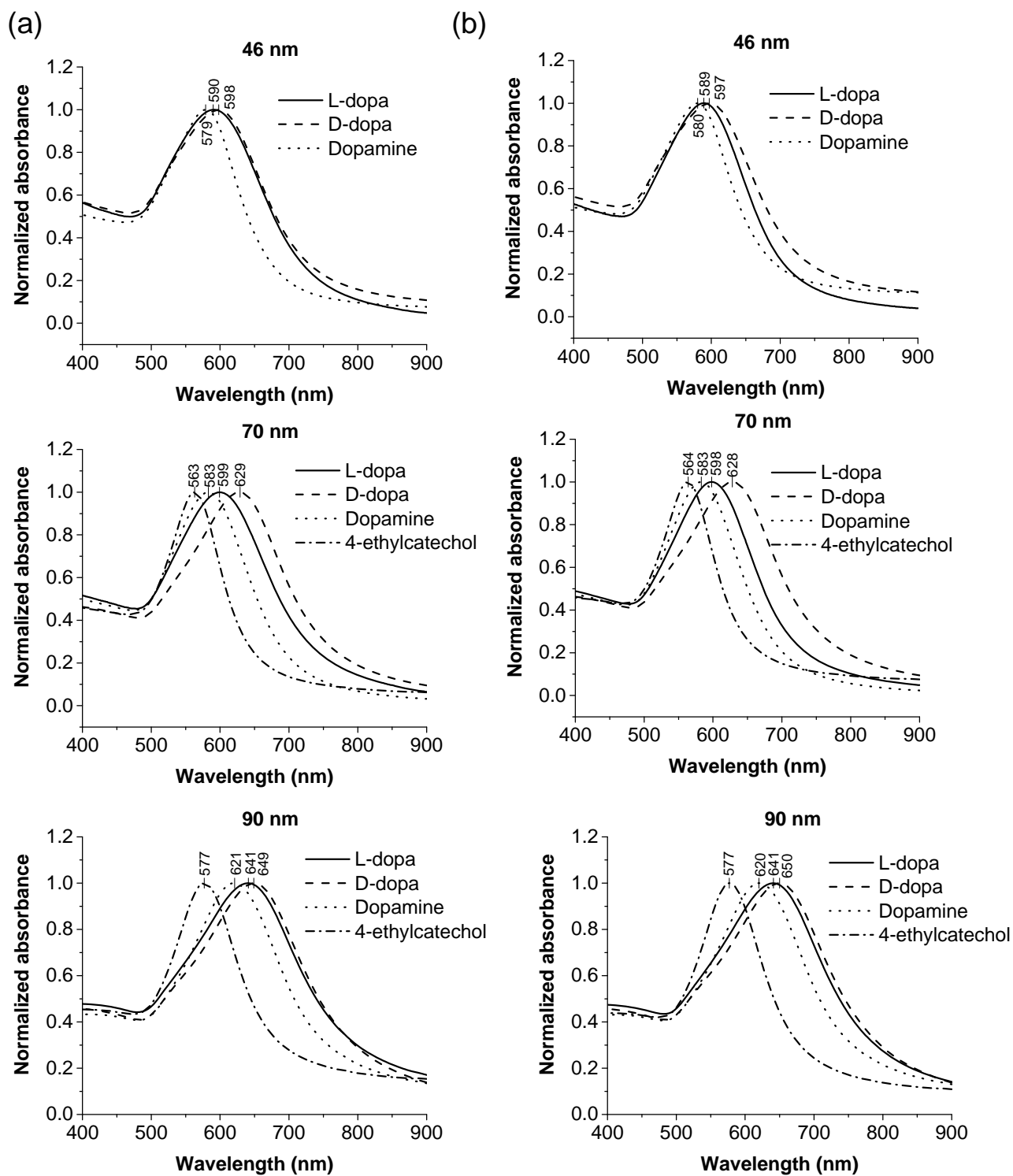


Figure S2. UV-vis absorption spectra of catechol functionalized AuNFs in (a) deionized water and (b) $1 \times$ PBS.

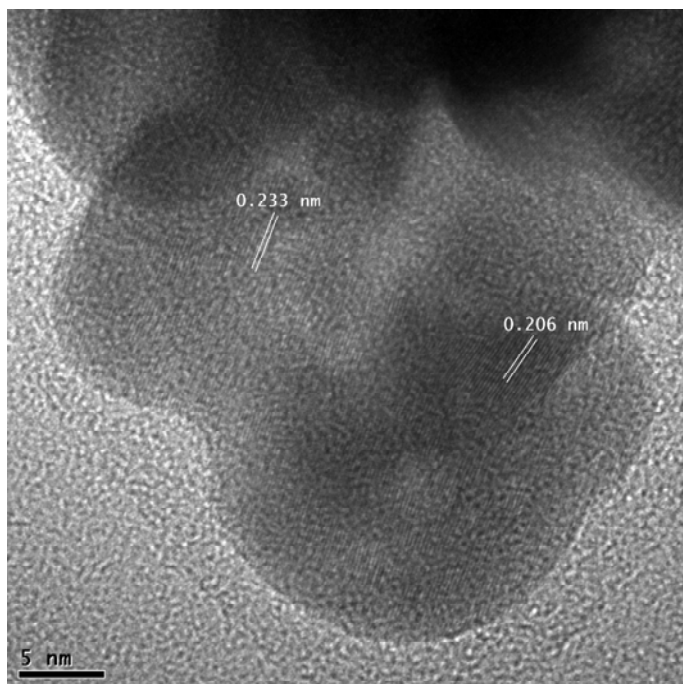


Figure S3. High resolution TEM (HRTEM) image of 90 nm L-dopa functionalized AuNF showing crystal lattice spacing characteristic of Au.

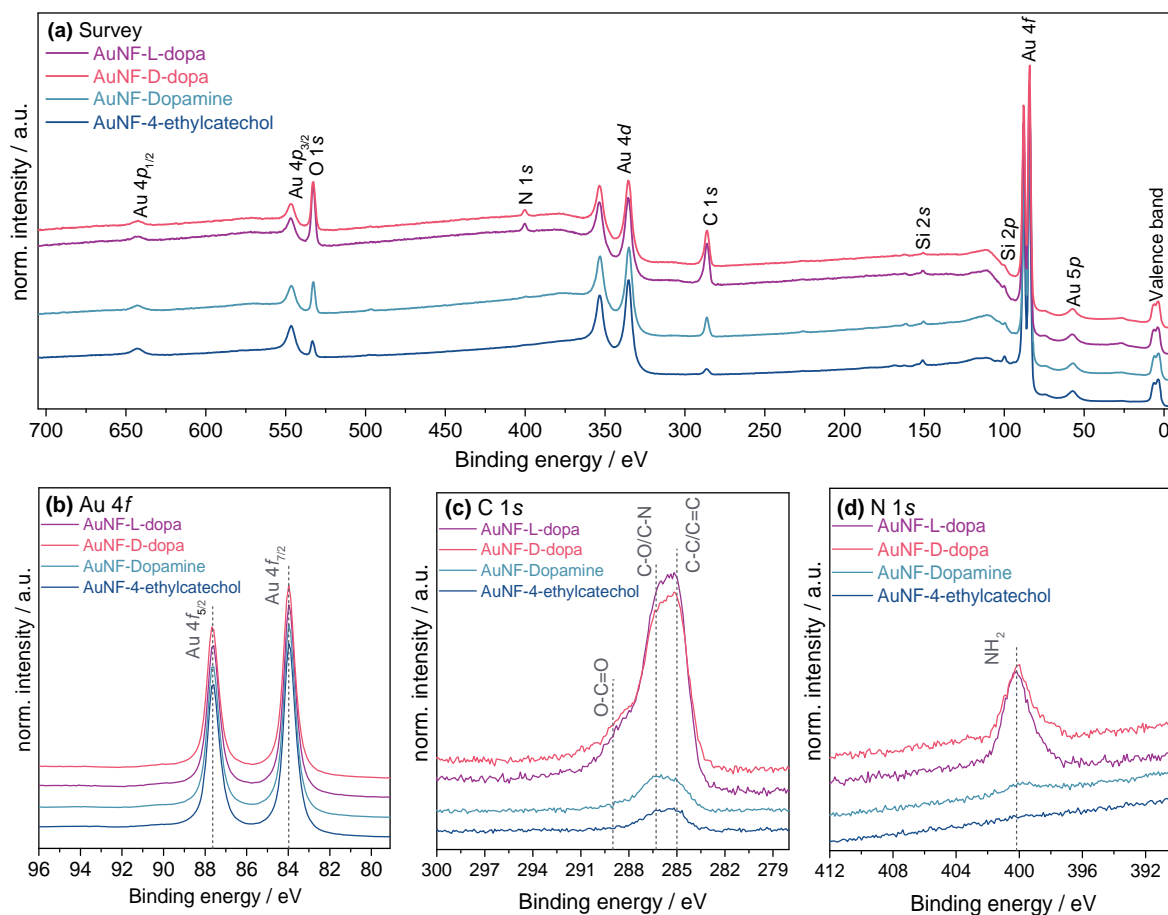


Figure S4. X-ray photoelectron spectroscopy (XPS) spectra obtained for various functionalized AuNFs, including (a) survey spectrum indicating all core levels as well as (b) Au 4f, (c) C 1s, and (d) N 1s core level spectra.

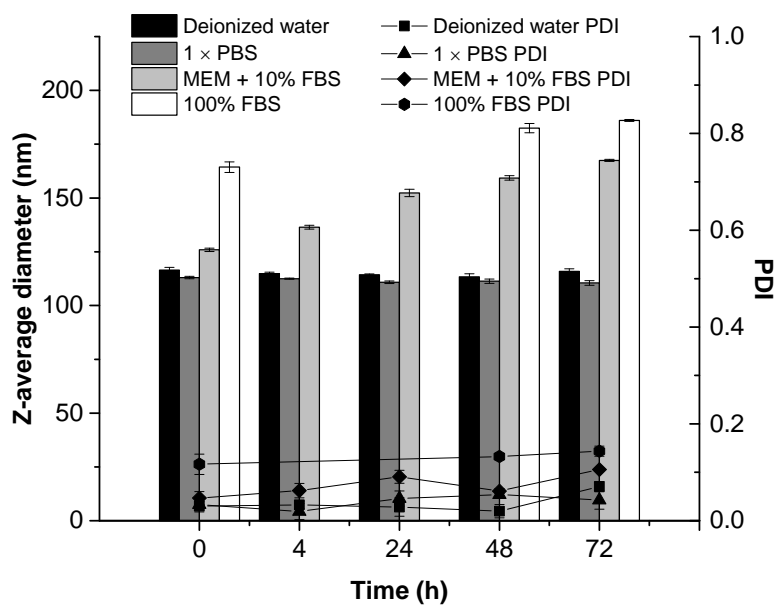
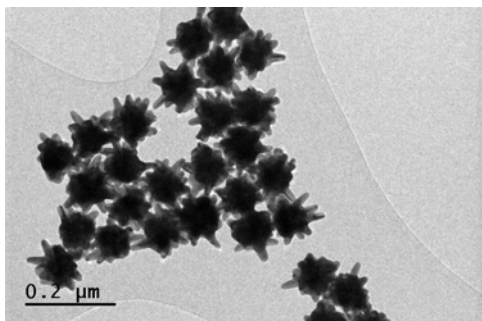


Figure S5. Stability of L-dopa-functionalized AuNFs in various biologically relevant media with shaking at 37 °C over time.

(a)



(b)

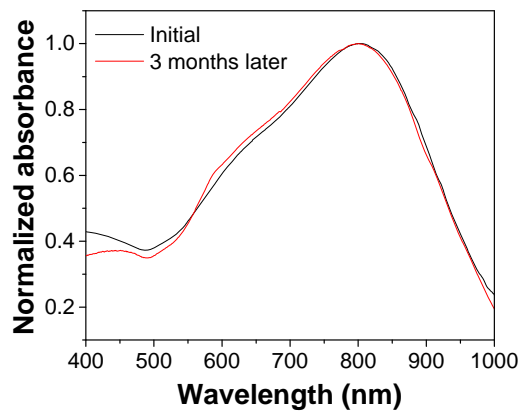


Figure S6. (a) TEM image of 4-ethylcatechol functionalized AuNUs used as non-targeting control in the photothermal ablation of breast cancer cells. (b) UV-vis spectrum demonstrating stability of the AuNUs upon storage at 4 °C for 3 months.

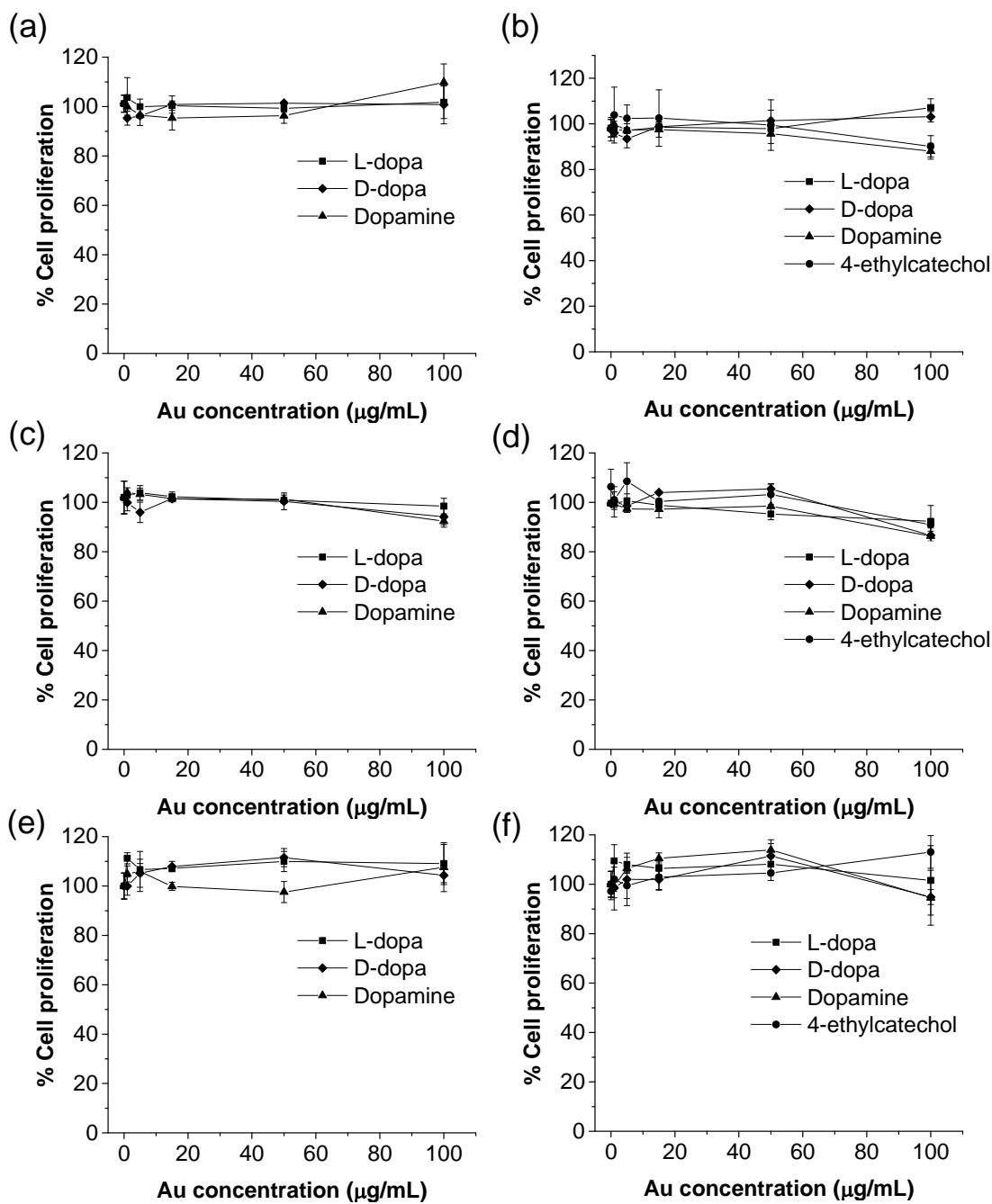


Figure S7. Cell viability of (a-b) MCF-7, (c-d) MDA-MB-231, and (e-f) MCF-10A treated with 46 nm (a, c and e) and 70 nm (b, d and f) functionalized AuNPs determined using WST-1 assay.

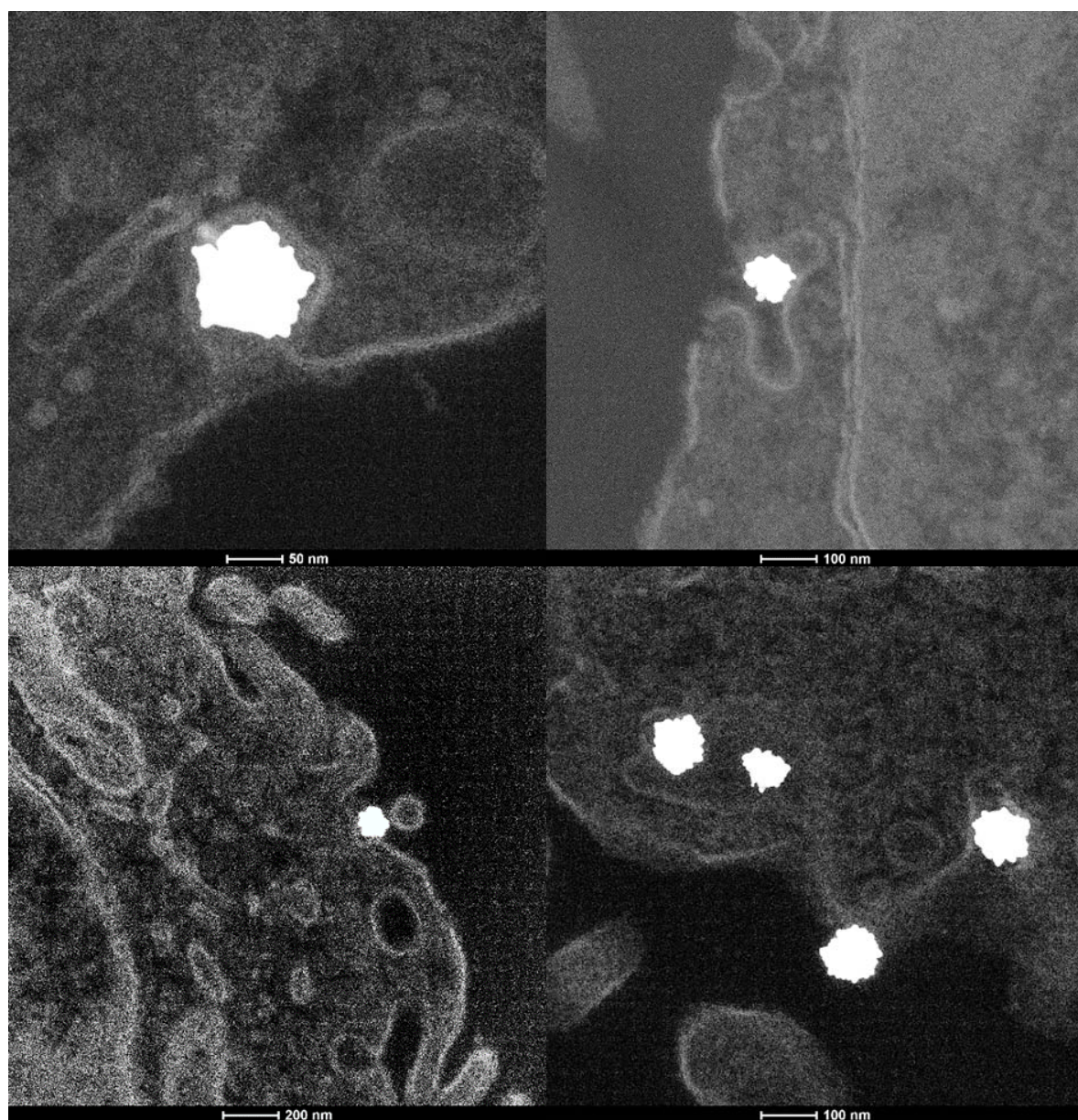


Figure S8. Additional HAADF-STEM images showing endocytic uptake of 90 nm L-dopa functionalized AuNF by MDA-MB-231.

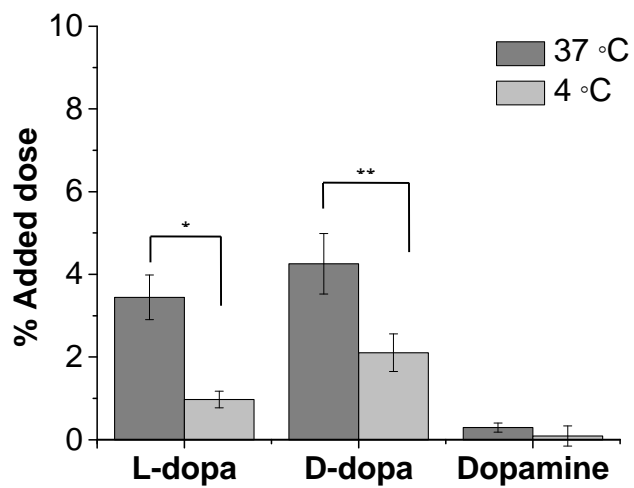


Figure S9. Temperature-dependent uptake of 90 nm functionalized AuNFs by MDA-MB-231 cells during 4 h incubation. * $P < 0.01$; ** $P < 0.05$.

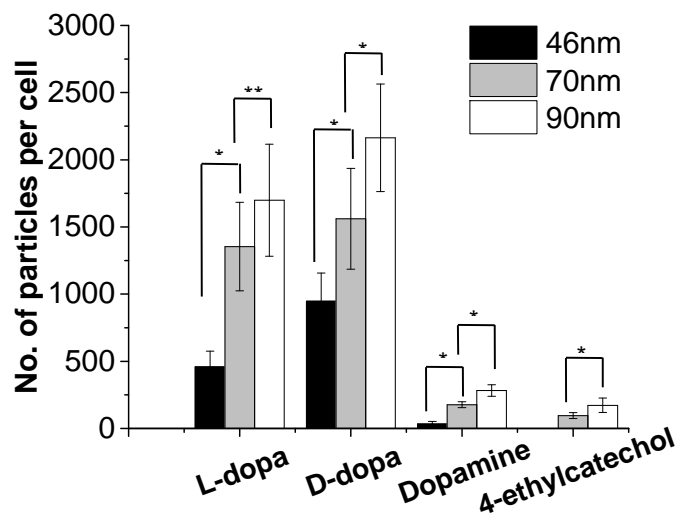


Figure S10. Size-dependent uptake of functionalized AuNFs by the MDA-MB-231 cell line during the 12 h incubation. * $P < 0.01$; ** $P < 0.05$.

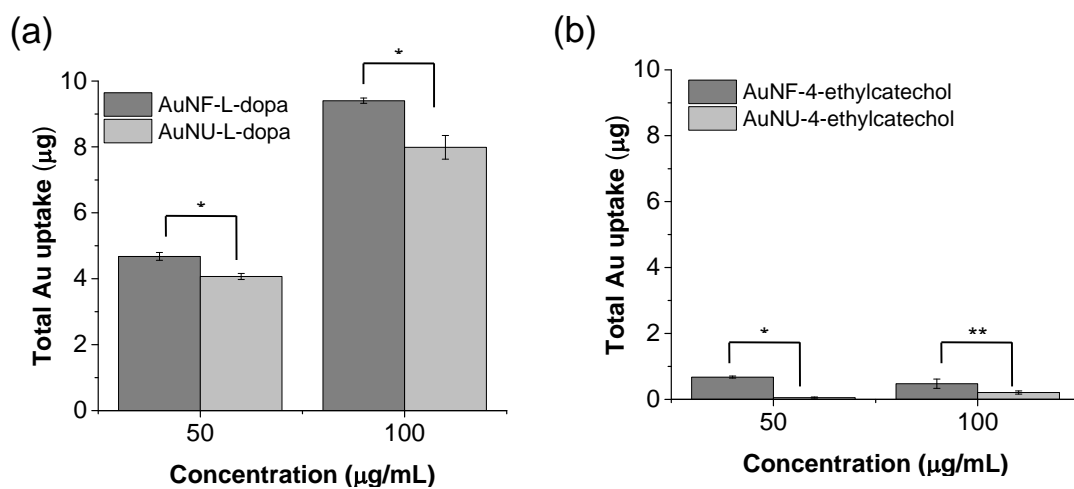


Figure S11. Effect of ‘nanoflower’ (AuNF) vs. ‘nanourchin’ (AuNU) morphology for cellular uptake of nanoparticles functionalized with (a) L-dopa, and (b) 4-ethylcatechol by MDA-MB-231. * $P < 0.01$; ** $P < 0.05$.

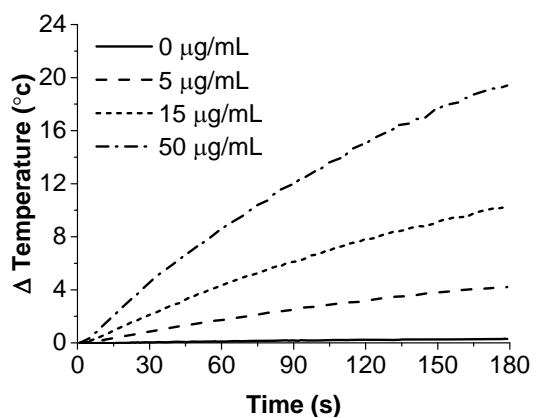


Figure S12. Thermal profiles of 4-ethylcatechol functionalized AuNUs at various concentrations under laser irradiation.

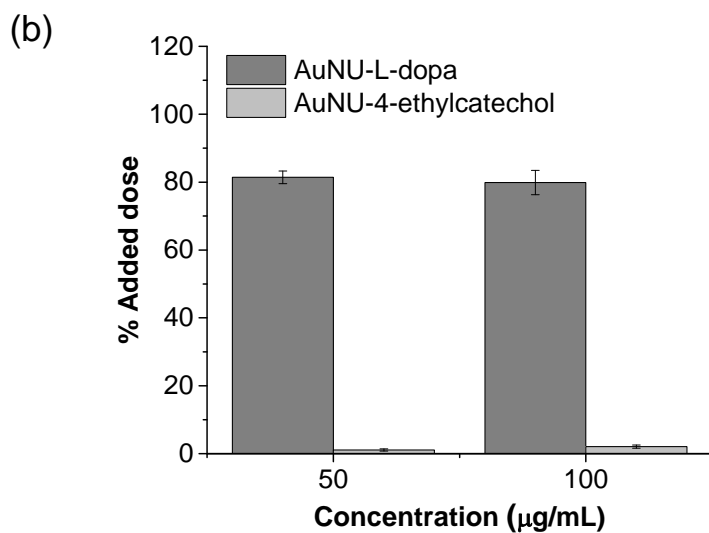
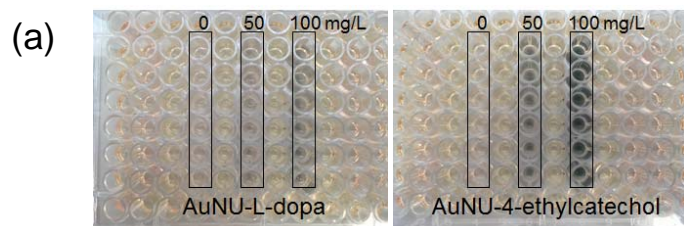


Figure S13. (a) Appearance of sea urchin-like AuNPs (AuNU) dispersions in the tissue culture well plates and (b) quantification of intracellular Au content after treatment of MDA-MB-231 with the indicated concentration of L-dopa and 4-ethylcatechol functionalized AuNUs for 72 h.

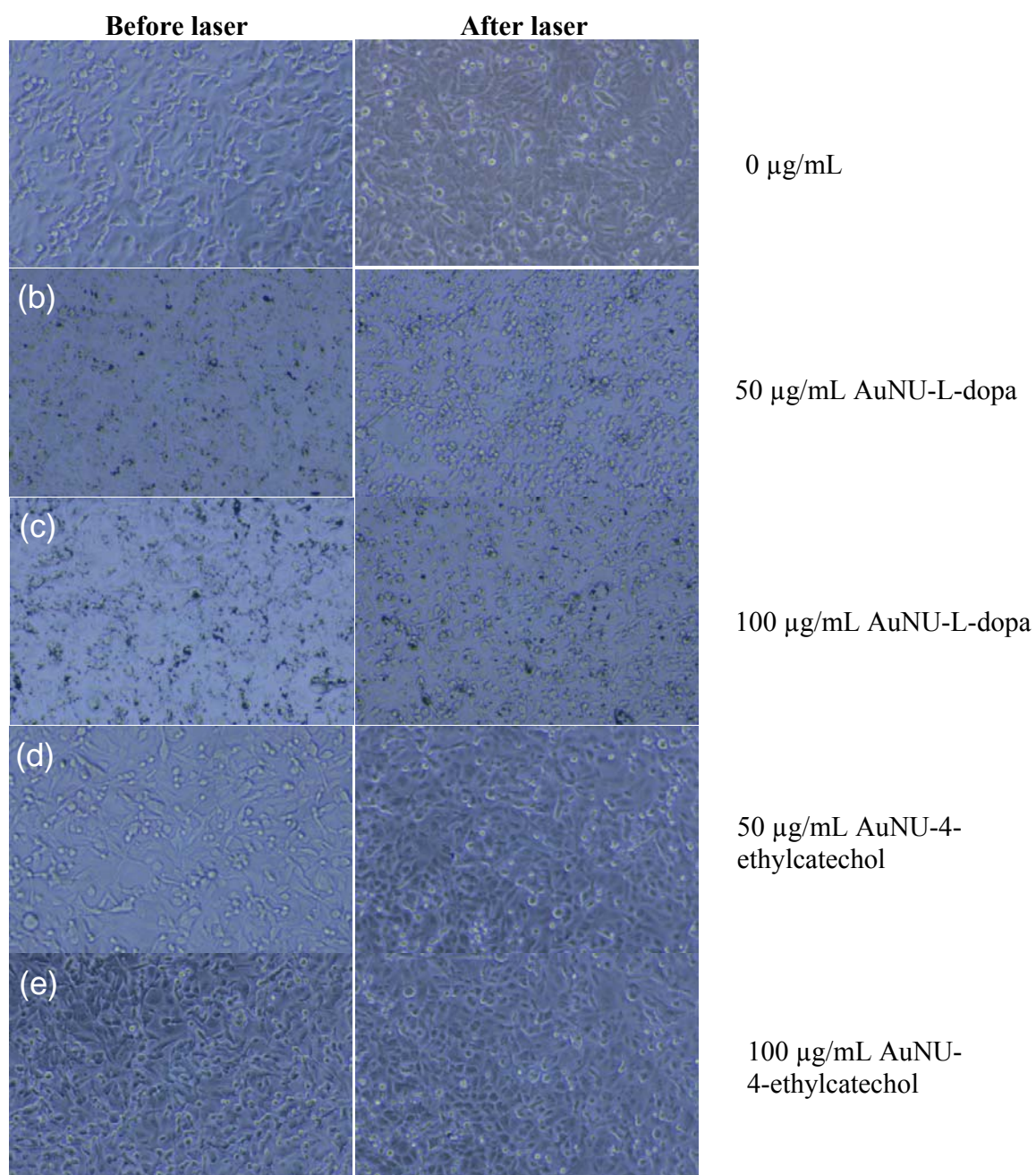


Figure S14. Bright-field optical micrographs of MDA-MB-231 cells pre-treated with (a) 0, (b) 50, and (c) 100 $\mu\text{g/mL}$ of L-dopa functionalized AuNUs as well as (d) 50 and (e) 100 $\mu\text{g/mL}$ of 4-ethylcatechol functionalized AuNUs before and after laser irradiation.